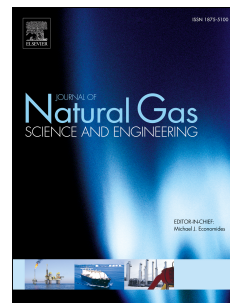


Journal Pre-proof

Amino functionalized ZIF-90@GO/MDEA nanofluid: As a new class of multi-hybrid systems to enhance the performance of amine solutions in CO₂ absorption

Mohammad Hadi Ghasemi, Vahid Irani, Ahmad Tavasoli



PII: S1875-5100(19)30362-2

DOI: <https://doi.org/10.1016/j.jngse.2019.103110>

Reference: JNGSE 103110

To appear in: *Journal of Natural Gas Science and Engineering*

Received Date: 13 October 2019

Revised Date: 28 November 2019

Accepted Date: 13 December 2019

Please cite this article as: Ghasemi, M.H., Irani, V., Tavasoli, A., Amino functionalized ZIF-90@GO/MDEA nanofluid: As a new class of multi-hybrid systems to enhance the performance of amine solutions in CO₂ absorption, *Journal of Natural Gas Science & Engineering*, <https://doi.org/10.1016/j.jngse.2019.103110>.

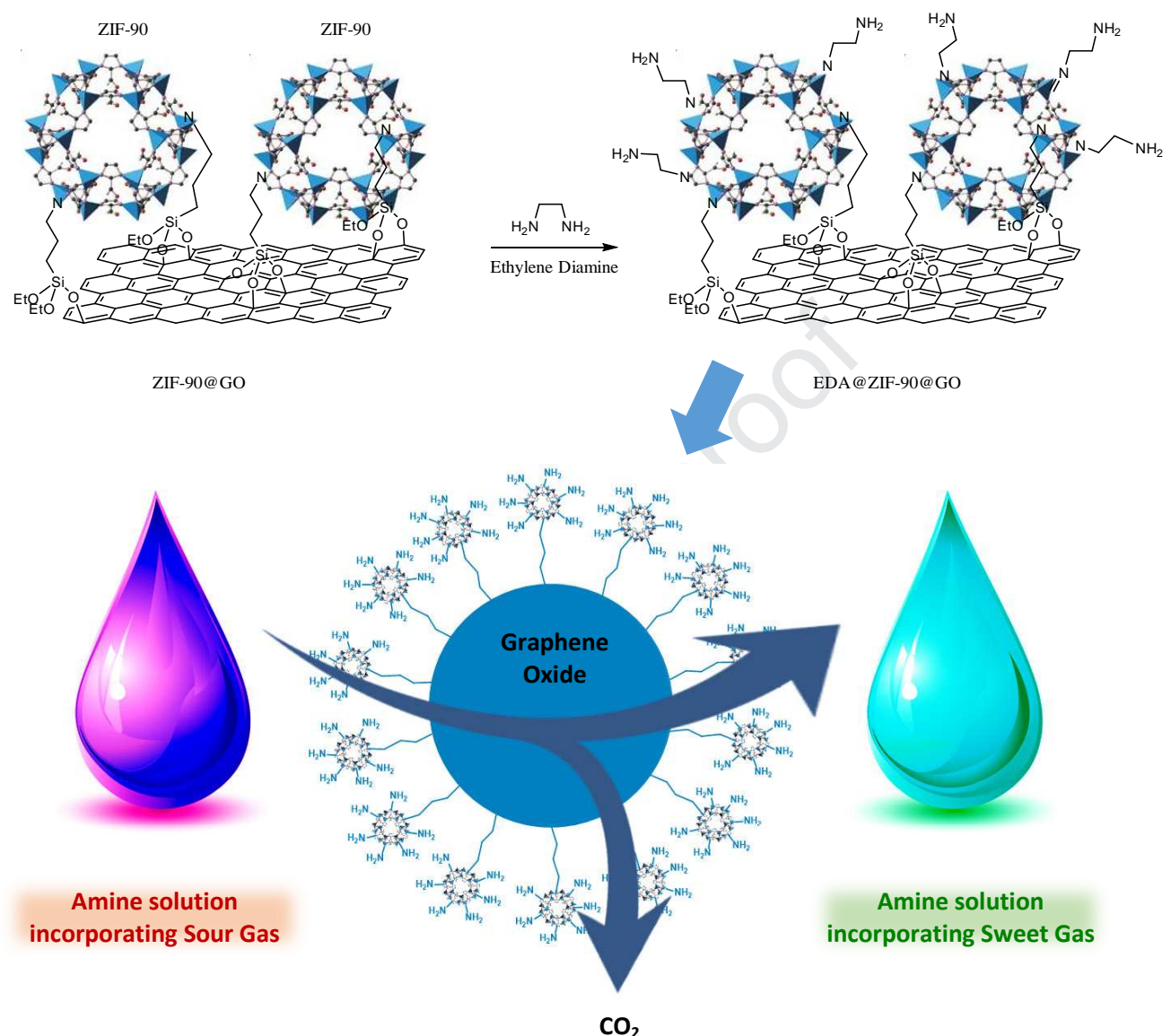
This is a PDF file of an article that has undergone enhancements after acceptance, such as the addition of a cover page and metadata, and formatting for readability, but it is not yet the definitive version of record. This version will undergo additional copyediting, typesetting and review before it is published in its final form, but we are providing this version to give early visibility of the article. Please note that, during the production process, errors may be discovered which could affect the content, and all legal disclaimers that apply to the journal pertain.

© 2019 Elsevier B.V. All rights reserved.

Mohammad Hadi Ghasemi.: performing the experiments and synthesis,
Editing

Vahid Irani: Investigation, Writing, performing the experiments and synthesis.

Ahmad Tavasoli: Conceptualization, Methodology, Supervision

Graphic Abstract

Journal Pre-proof

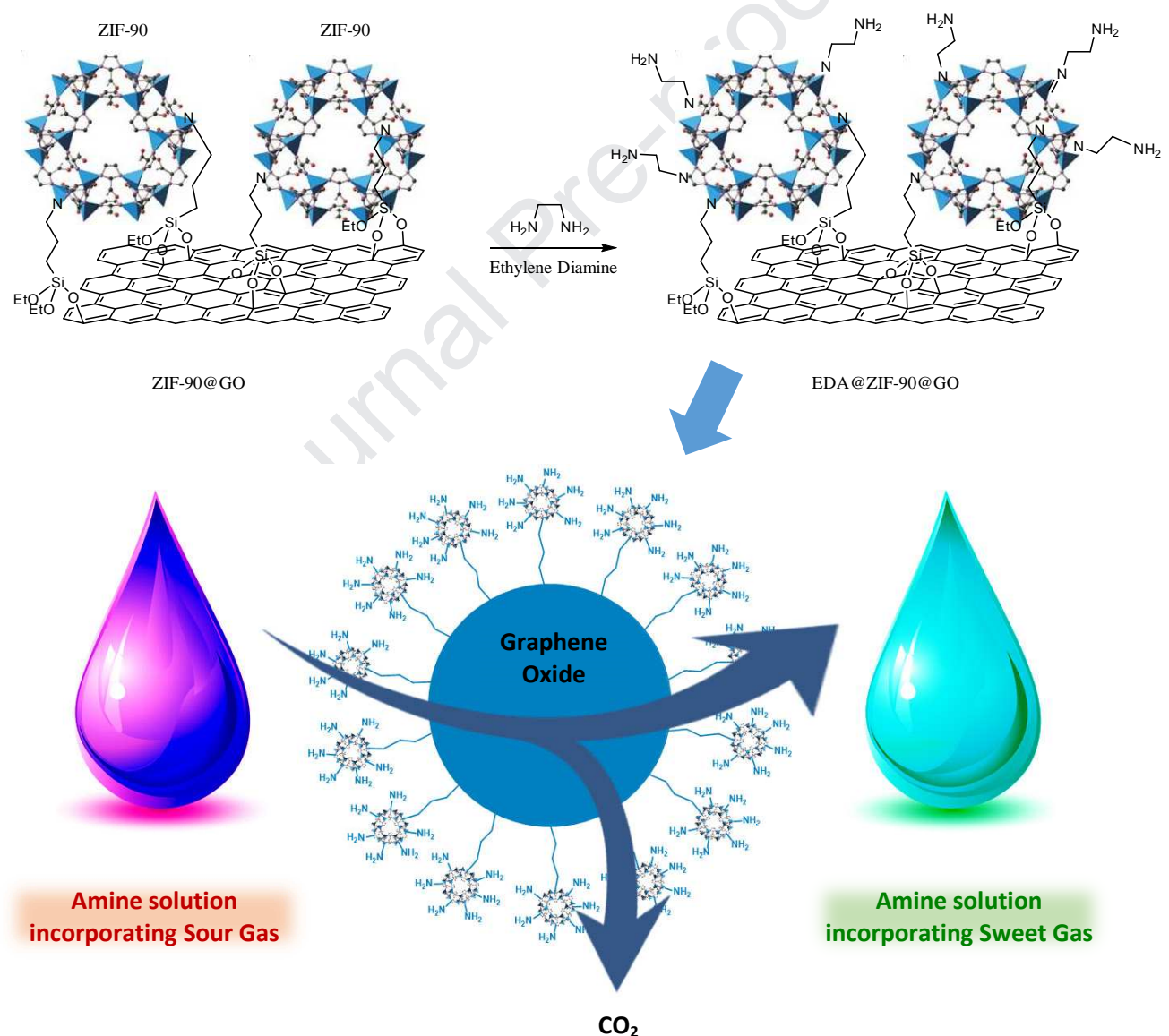
Amino functionalized ZIF-90@GO/MDEA nanofluid: As a new class of multi-hybrid systems to enhance the performance of amine solutions in CO₂ absorption

Mohammad Hadi Ghasemi, Vahid Irani, Ahmad Tavasoli*

University of Tehran, College of Science, School of Chemistry, Tehran, Iran.

* Corresponding author: Email: tavasoli.a@ut.ac.ir, Phone: (+98)-21-61113643, Fax: (+98)-21-66495291

Graphic Abstract



Abstract

Global climate change has enforced a critical action to mitigate carbon emissions. In this study, a novel procedure was investigated by addition of amine-functionalized graphene oxide into methyldiethanolamine (MDEA) to improve the CO₂ absorption capacity. The nanocomposite EDA@ZIF-90@GO was prepared by incorporation of (3-Aminopropyl) triethoxysilane (APTES) onto the graphene oxide surface and consequently functionalization of as-prepared nanostructure with ZIF-90 as well as ethylenediamine (EDA). This reagent was utilized because of various functional groups, high surface area, and potential surface modification. The stability of nanofluid was measured by zeta potential analysis. Firstly, we studied the nanoparticle loading using MDEA based nanofluid containing different dosages of GO to reach the optimal concentration. The results revealed an absorption enhancement of 9.1% and 10.4% for dosages of 0.1 wt.% and 0.2 wt.%, respectively. Then, after the addition of 0.1 wt.% EDA@ZIF-90@GO to amine solution, the CO₂ absorption was enhanced up to 23%. Different partial pressure and temperatures were employed and the results showed that the temperature has a negative effect on the performance of the system, while increasing the CO₂ partial pressure led to an increase in absorption capacity rate. Thermal gravimetric analysis (TGA) confirmed the reusability of the nanofluid due to the high temperature needed for the decomposition of functional groups. Thermal conductivity and convective heat transfer coefficient were improved after addition of the nanoparticles into the base fluid.

Keywords: Nanofluid; CO₂ Absorption; Nanocomposite; Graphene Oxide, Metal-Organic Framework

1. Introduction

CO₂ is known as a major greenhouse gas in global warming. It is believed that its atmospheric concentration is going to be a critical issue in the industrial world and will reach 550 ppm by 2050 [1,2]. This increasing of CO₂ concentration resulting in an increase of global warming concerns. So, the mitigation of CO₂ emissions has received attention from various researchers around the world [3–6]. Different CO₂ removal procedures have been utilized, among which aqueous amine solution is a common method for this purpose [7]. Amine solvents show high performance at atmospheric pressure. This method is well known for the absorption of CO₂ in different processes performing at atmospheric conditions such as post-combustion processes [7–9]. The most prevalent alkanolamines used in the acid gas absorption process are monoethanolamine (MEA), N-methyl-diethanolamine (MDEA), diethanolamine (DEA), triethanolamine (TEA) and diglycolamine (DGA). Among them, MDEA has been widely used because of some properties (e.g. carbamate formation and low corrosion rate in comparison with other alkanolamines) [10–14]. In the case of reactivity, MDEA has a lower performance relative to DEA and MEA, but CO₂ loading capacity has been reported to be definitely higher. The common dosage of MDEA aqueous solution is in the range of 40-45 wt.% [15].

However, alkanolamines suffer from several disadvantages including poisonous quality, degradation, volatility, the move of water into the gas flow during the process and high vitality required for the regeneration process [16]. Furthermore, this technique requires high energy levels and causes extreme corrosion in the equipment and should be improved. In order to overcome these problems, solid sorbents are a promising and alternative method without the mentioned disadvantages. Solid sorbents with chemisorption or physisorption interactions have been widely employed in recent years [17–20]. Many solid sorbents have been studied such as metal-organic frameworks (MOFs) [21], carbons [22], zeolites [23], covalent organic frameworks (COFs) [24] and amine-modified porous solids [25]. From the many proposed solid sorbents, carbonaceous materials have played a significant role in efficient CO₂ capture due to the high surface area, the lower energy requirement for regeneration and suitable thermal stability. Activated carbon, carbon nanotube (CNT) and graphene oxide are the most used support for CO₂ capture. Carbon-based sorbents will be less affected by moisture available in the feed due to the hydrophobic properties of microporous carbon-based materials [26,27]. The adsorption ranges of carbon materials prepared from different methods are 0.5-6.5 mmol/g at ambient conditions [28].

Amine modified solid sorbents are a promising low energy consumptive material for different CO₂ capture purposes. Carbon-based materials are widely used traditionally in different adsorption processes such as gas capturing and wastewater treatment [29]. Graphene oxide shows a favorable performance for removal of various elements including heavy metals some radioactive elements due to its applicable surface and presence of many functional groups such as carboxyl, hydroxyl, carbonyl, and epoxide groups [27]. GO has been widely employed as a support in different industrial processes because of important features such as chemical stability, non-toxicity, and low-cost preparation procedure. The adsorption ability of GO can be improved by decorating nitrogen-containing ligands and functional groups on the surface of the as-prepared GO [30].

MOFs are known as a new class of sorbent materials due to large porosity properties, high surface area as well as tunable pore size available in their network. Their performance can be improved through some modification processes such as a combination of these materials with porous carbon and graphene. GO surface properties can be modified through including various procedure to enhance the capability of the GO in gas adsorption and removal of heavy metals processes [31,32]. NH₂-rich cross-linkers and polymers are usually applied and grafted on the surface. Recently, various studies have been conducted on the preparation of GO-based composites. MOF/GO composites have been evaluated in different processes such as gas adsorption, catalysis, and other pollutant adsorption. However, the gas adsorption capacity of these materials is somewhat low, so a hybrid method is required for overcoming the limitations [33].

Combination of tow above-mentioned methods as amine-based nanofluids is a promising procedure to enhance the absorption capacity and decrease required energy costs. These nanofluids are prepared by dispersing nanoparticles (1-100 nm) into base fluid and exhibit superior thermal conductivity than base fluid. Various studies have reported a mass transfer enhancement in nanofluid because of the presence of nano-sized particles [34,35].

In this study, a novel composite was synthesized through various modifications on the surface of GO. Graphene oxide was functionalized with APTES to incorporate NH₂ groups on the surface. Then, ZIF-90@GO composite was prepared and functionalized with EDA to study the CO₂ absorption properties of methyl diethanolamine (MDEA) before and after addition of synthesized nanocomposite. 0.1 wt.% EDA@ZIF-90@GO was added into 40 wt.% aqueous MDEA solution to study the absorption capacity.

2. Experimental

2.1 Materials

Methyldiethanolamine (>99%, Merck), CO₂ gas (99%, Roham gas company), (Graphite powder, Zinc nitrate tetrahydrate (>99%, Merck), Potassium permanganate, Imidazolate-2-carboxaldehyde (ICA; >99%, Aldrich), 3-Aminopropyltriethoxysilane (APTES; 98%, Aldrich), Ethylenediamine (Aldrich), Hydrogen peroxide (Merck), Hydrochloric acid (Merck), Sodium nitrate (Merck), Methanol (Aldrich), Toluene (ACROS) and N,N-dimethylformamide (DMF, ACROS). All chemical used in this study were analytical grade without further purification.

2.2 Preparation of GO

GO was synthesized through a modified Hummers method [36]. Briefly, 2 g graphite powder (mesh 500) was added to 50 ml concentrated sulfuric acid under stirring condition. Then, 2 g sodium nitrate was added to the solution followed by stirring at 0 °C for an hour. 7.3 g KMnO₄ was slowly added to the mixture and stirred for 2 hours. Afterward, the temperature was raised to 35 °C and stirred for 2 hours. 46 ml distilled water was added along with increasing the temperature to 90 °C and the mixture was stirred for 30 min. Finally, the reaction was stopped by addition of 140 ml distilled water and 16 ml H₂O₂ (30%). The as-prepared suspension was maintained under ultrasound condition (35 kHz) for 30 min. The obtained GO was washed with diluted HCl and distilled water several times. The dark brown precipitate was dried in a vacuum oven at 40 °C for 24 hours.

2.3 Preparation of ZIF-90

ZIF-90 was synthesized through the solvothermal method [37]. In this regard, 0.21 mole Zn(NO₃)₂.4H₂O and 0.30 mole imidazolate-2-carboxaldehyde were dissolved in 3 ml DMF and heated at 100 °C for 18 hours. Then, the solution was filtered and obtained precipitate was washed with methanol several times and then dried at the oven. A schematic of the reaction is presented in Fig. 1.

Fig. 1

2.4 Functionalization of GO with APTES

To anchor the APTES on the surface of GO, a method was employed by changing the support. 0.2 g GO was added to a twin-necked round-bottom flask which was equipped to a

stirrer. Then, 1 ml 3-aminopropyltriethoxysilane (APTES) and 10 ml toluene was added and the mixture was left at 110 °C for 2 hours. Afterward, the mixture was cooled down and filtered by methanol to remove the unreacted APTES. Finally, APTES functionalized GO was dried in a vacuum oven to obtain 0.4 g APTES functionalized GO [38]. A schematic of the process is presented in Fig. 2.

Fig. 2

2.5 Preparation of ZIF-90 functionalized GO

To prepare ZIF-90@GO, some modifications were applied to the solvothermal method used in the literature [32]. In a 50 ml stainless steel autoclave equipped with internal Teflon insulation, 0.2 g APTES functionalized GO and 0.1 g ZIF-90 was added to 10 ml DMF and solution was maintained at 100 °C for 18 hours. When the reaction was completed, the mixture was filtered several times by DMF and methanol. The as-prepared mixture was dried at 60 °C for 8 hours. The process is schematically presented in Fig. 3.

Fig. 3

2.6 Preparation of EDA functionalized ZIF-90@GO

In this step, the as-prepared ZIF-90@GO was functionalized with EDA. For this purpose, some slight modifications were applied to the procedure reported in the literature [39]. First, in a 25 ml round-bottom flask equipped with a stirrer, 0.1 g ZIF-90@GO, and 1 ml EDA was added to 10 ml tetrahydrofuran (THF) and the obtained mixture was refluxed at 50 °C for 4 hours. Then, the mixture was washed with methanol several times and dried in a vacuum oven at 60 °C over a night. The procedure is shown in Fig. 4.

Fig. 4

2.7 Preparation of nanofluid

First, a 40 wt.% aqueous MDEA solution was prepared by addition of 40 ml MDEA into 60 ml deionized water. Then, 0.1 wt.% as prepared nanostructure was added into the solution. To stabilize the nanoparticles added into the solution, the as-prepared nanofluid was maintained in an ultrasonic bath for 1 h. Apparatus and procedure

2.8 Apparatus and procedure

2.8.1. Gas absorption apparatus and method

Briefly, a two-wall equilibrium cell equipped to a stirrer was employed to measure the carbon dioxide absorption at different temperatures and pressures. A water bath (which was equipped to a pump) was employed for circulation of a fluid in the external wall of the equilibrium cell to adjust temperature as desired. Temperature stability of the measurements was within ± 0.02 K by employing a TM-917 Lutron digital thermometer with an accuracy of 0.01 K. A sensor (Pt-100w) were placed in the cell to control and measure the temperature. Two digital pressure gauge was used to measure the gas container and equilibrium cell pressure. A digital pressure gauge (Baroli BD sensors) within a range between 0-40 bar with 0.1% of full-scale accuracy was placed on the equilibrium cell to determine the partial pressure of the cell. A gas container with a well-known volume was utilized to after the gas cylinder and before the equilibrium cell for introducing a known amount of gas into the equilibrium cell. Another digital pressure gauge (Baroli BD sensors) in the range of 0-60 bar with 0.1% of full-scale accuracy was placed to determine the pressure of the gas container. In fact, gas container plays a critical role in calculation of gas amounts introduced to the system via some calculations that has been presented. Knowing the precise pressure amount employed on the gas container and cell in order to measure the absorbed gas. The unknown volumes were determined using pressure-swing-experiments (PSE) method [40–42]. This method is based on the Charles-Gay-Lussac law so that the unknown volume is measured by difference in initial and final pressures between an unknown volume container and well-known volume container.

The operation of the system was carried out in such a way that first, a vacuum was applied to the equilibrium cell via vacuum pump system in order to devoid the gas tank and equilibrium cell from any impurity gas. Then, desired and certain amount of prepared mixed amine solution was introduced to the equilibrium cell. In order to obtain the equilibrium state, the system temperature was set on the desired value. Then, after introducing the CO₂ to the equilibrium cell from the gas container with volume of 309.45 ml, and obtaining equilibrium state, the pressure was recorded via pressure sensor. The amount of CO₂ introduced into the equilibrium cell was calculate by an available procedure Hosseini Jenab et al [43,44]and Park and Sandall [45]. The detailed PVT data was obtained from the National Institute of Standards and Technology that provides data for all fluids including pure CO₂

$$n_{CO_2} = \frac{V_C}{RT_a} \left(\frac{P_1}{Z_1} - \frac{P_2}{Z_2} \right) \quad (1)$$

Where V_c denotes the volume of the CO₂ container. T_a is temperature of CO₂ container (ambient temperature) and R is universal gas constant, Z₁, Z₂ present the compressibility factors corresponding to initial and final state in gas container before and after gas introducing. P_{CO₂} (Equilibrium partial pressure of CO₂ in the gas phase of the equilibrium cell) was calculated by

$$P_{CO_2} = P_T - P_V \quad (2)$$

Where P_T demonstrate the total absolute pressure and P_V denotes the vapor pressure of solution after reaching stable state in equilibrium cell, at low temperatures MDEA has low vapor pressure, so in this work the vapor phase of MDEA were neglected. The amount of remaining CO₂ in the gas phase was calculated by

$$n_{CO_2}^g = \frac{V_g P_{CO_2}}{Z_{CO_2} RT} \quad (3)$$

Where V_g is the gas phase volume in the equilibrium cell, Z is the compressibility factor of CO₂ at related P and T, and T is temperature of the equilibrium cell. The moles of CO₂ in the liquid phase was determined from

$$n_{CO_2}^l = n_{CO_2} - n_{CO_2}^g \quad (4)$$

And eventually, CO₂ loading in the liquid phase was calculated as

$$m_{CO_2} = \frac{n_{CO_2}^l}{w_{sol}} \quad (5)$$

In which w_{sol} is the mass of solvent in kg. The exact volume of gas phase, V_g, is the difference between the cell volume and uncharged solvent volume. The errors were determined and then the uncertainties were estimated using literature.

A schematic structure of the system including the equilibrium cell, gas container, gas reservoir, water bath, and estimation instruments has been exhibited in Fig. 5.

Fig. 5

2.8.2. Thermal conductivity and convective heat transfer apparatus and method

Thermal conductivity was investigated using a KD2 Pro thermal analyzer obtained from Decagon, USA. In this method, according to the transient hot wire, the thermal conductivity

was analyzed through the response (temperature/time) received from the probe with 60 mm length and 1.3 mm diameter which was obtained by an abrupt electrical pulse and deactivation of Fourier's law and temperature. Before any measurement, the calibration of the samples was conducted using deionized water and consequently the probe was remained for 20 min at a constant temperature. Thermal conductivity of the samples was measured at 298, 308 and 318 K. The KD2 Pro device was equipped to a circulator for controlling the temperature and the enhancement rate was calculated by the following equation:

$$\text{enhancement rate\%} = \frac{K_n - K_f}{K_f} \times 100 \quad (6)$$

Where K_f and K_n are the thermal conductivity of the base fluid and nanofluid, respectively.

The convective heat transfer coefficient was measured using a system depicted in Fig. 6. As shown, the system consists of different parts including testing chamber, pump, reservoir, exchanger and a circulator. In the testing chamber, a copper tube with 1m length and 11.42 mm diameter is inserted. As shown in Fig. 6, five thermocouples (K-type) were fixed at different places along the tube and the inlet and outlet of the testing part were controlled by two thermocouples (K-type). So, the convective heat transfer coefficient was determined by the following equation:

$$h(x) = \frac{q^0}{T_s(x) - T_m(x)} \quad (7)$$

where $T_m(x)$ is referred to the temperature of the fluid on the tube, $T_s(x)$ is related to the temperature of the tube wall, $h(x)$ is known as the convective heat transfer coefficient, q^0 is referred to the heat flux and $\Delta T = T_s(x) - T_m(x)$ is the temperature difference between the solid surface and the surrounding fluid area. The experiments were conducted by warming up the system by a heater and the pump was used for circulation the fluid to remove the bubbles. Then, temperature and flow rate was adjusted to reach a stable state in the system. Afterward, the data was obtained and the average convective heat transfer coefficients were calculated.

Fig. 6

2.9 Characterization

Analysis of functional groups available on the surface of the nanoparticles was performed by BRUKER EQUINOX55 using KBr pellets for all the powders. Morphology of nanoparticles

was determined using a scanning electron microscope (SEM, MIRA3 TESCAN) operated at 15 kV. Brunauer-Emmett-Teller (BET) analysis was performed on ASAP-2000 to find out the porosity and surface area. First, nanoparticles were degassed and then the analysis was employed using N₂ gas flow. X-ray diffraction (XRD) were recorded on Phillips PW1800 diffractometer (40 kV, 30 mA). Thermogravimetric analysis (TGA) were conducted with a Perkin-Elmer Pyris 1 TGA. The stability of nanofluids was examined by zeta analyzer from the SZ-100 HORIBA scientific instrument.

3. Results and discussion

3.1 Characterization

The stability of nanofluid was investigated by zeta potential analysis. High zeta potential values (more than ± 25 mv) confirm the desired stability related to the prepared nanofluid [46]. By performing the zeta potential analysis, a -39.4 mV was obtained so that revealed the desired stability of nanofluid. The zeta potential diagram is presented in Fig. 7.

Fig. 7

As shown in Fig. 8, the XRD patterns of ZIF-90, GO, ZIF-90@APTES-GO and EDA@ZIF-90-GO have been presented, respectively. The featured peak at $2\theta=9.8^\circ$ is related to (001) plane for GO crystalline structure. After modification or functionalization, this featured peak shifts to lower angles because of intercalation of amine groups leading to an increase in the GO interlayer spacing. The XRD pattern of as-synthesized ZIF-90 shows different planes that are in agreement with data available in the literature. XRD patterns of ZIF-90@APTES-GO and EDA@ZIF-90@GO show decreased intensities compared with the pristine GO and ZIF-90 due to the coverage of functionalization groups [33,47].

Fig. 8

Fig. 9 presents the FTIR spectra of GO, APTES-GO, ZIF-90@APTES-GO, and EDA@ZIF-90@APTES-GO. Hydroxyl groups (3384 cm^{-1}), epoxy groups (1239 cm^{-1}), carboxyl groups (1725 cm^{-1}), aromatics (1631 cm^{-1}) and alkoxy groups (1070 cm^{-1}) confirms the functional groups on the surface of GO which show a desirable agreement with the data reported in the literature. In the case of APTES-GO, a new featured peak located at 1100 cm^{-1} appeared which is corresponded to the O-Si functional groups formed after modification of GO with APTES. A specific peak located at 1638 cm^{-1} is related to the aromatics (C=C). In the case of ZIF-90@APTES-GO, the peaks appeared at 478 cm^{-1} and 1250 cm^{-1} are assigned to

stretching and bending of Si-O bond. The peak located at 1100 cm^{-1} also corresponds to the Si-OR bond. For EDA-ZIF-90@APTES-GO, a new peak is appeared at 1558 cm^{-1} confirming the presence of -CO-NH bonds [48].

Fig. 9

Fig. 10 shows the SEM images of the GO, APTES functionalized GO, ZIF-90@APTES-GO, and EDA-ZIF-90@APTES-GO, respectively. As shown, the pristine GO shows a less porous morphology before modification. In the case of ZIF-90, a rhombic morphology is observed. The surface is more porous than pristine GO after modification by APTES while some of the pores are blocked. When ZIF-90 was introduced on the surface, the porosity of the surface was a key characteristic of the as-synthesized nanocomposite. In this case, many pores are blocked after functionalization of ZIF-90 on the surface of the GO. The hydroxyl and carboxyl groups available on GO anchored the Zn from solution by coordination bonding [48–50].

Fig. 10

Fig. 11 shows the N_2 adsorption-desorption of ZIF-90@APTES-GO and EDA-ZIF-90@APTES-GO to study the BET surface area and pore size of samples. As shown, the surface area is reduced from $66.5\text{ m}^2/\text{g}$ in the case of ZIF-90@APTES-GO to $37\text{ m}^2/\text{g}$ in the case of EDA-ZIF-90@APTES-GO. This confirms the blocked pores after double modification of composite.

Fig. 11

Thermal behavior (TGA) of ZIF-90, GO, ZIF-90@GO and EDA@ZIF-90@GO are depicted in Fig. 12. In the case of GO, there is a weight loss (5%) observed at a temperature of $100\text{ }^\circ\text{C}$ which is attributed to the moisture evaporation. Another weight loss (%) occurred in the temperature range of $175\text{--}235\text{ }^\circ\text{C}$ due to the decomposition of oxygen-containing functional groups available on the surface of GO. After functionalization by ZIF-90, the as-prepared composite showed more thermal stability properties compared with pristine GO. The temperature ranges from 150 to $250\text{ }^\circ\text{C}$ is mainly related to the decomposition of oxygen groups. Formation of Si-O bonding stable due to the incorporation of APTES is known as the main reason for small weight loss relate to the GO. The more thermally stable structure was obtained while the composite was functionalized by EDA. As shown, the weight loss (10%) occurred at $150\text{--}175\text{ }^\circ\text{C}$ is mainly because of the decomposition of amine groups incorporated

on the surface of the composition. So, the composite showed a thermally stable property after modification by different groups [33,51]. From the literature, the desired temperature for regeneration of acid gas saturated MDEA solution has been reported to be at 130 °C. So, these results showed that the regeneration process could be performed successfully because of the thermal stability of amino groups grafted on the outside of the GO.

Fig. 12

3.2 Absorption experiments

The gas solubility measurements were conducted at different temperatures. To ensure the accuracy accompanied by the system, some validation experiments were carried out referring to the data available in the literature. For this purpose, a 30 wt.% aqueous MDEA solution was employed to measure the CO₂ solubility at 313.15 K according to the data reported by Shen et al [52]. Another validation test was performed to compare the obtained data with results reported by Ma'mun et al [53] at two different temperatures including 328.15 K and 343.15 K. As reported in Fig. 13 and 14, the validation results showed a good agreement with the data available in the previous works.

Fig. 13

Fig. 14

After confirming the system performance via validation test, solubility experiments on as-prepared nanofluid was conducted. A Pycnometer was utilized to investigate the density of prepared nanofluids. Densities were measured after addition of 0.1 wt.% nanocomposite into the aqueous MDEA at 303.15, 313.15, 323.15 and 333.15 K. The combined standard uncertainties of Pycnometer was provided to be 0.00025 g/cm³. The measured densities are reported in Table 1. As shown, densities decreased by increasing the temperature due to the relationship between volume and temperature.

Table 1. The measured densities of nanofluid at desired temperatures (combined standard uncertainties U_c(ρ)=0.00025 (g/cm³).

T (K)	ρ (40 wt.% MDEA + 0.1 wt.% EDA@ZIF-90@GO)
303.15	1.0401
313.15	1.0376

323.15	1.0264
333.15	1.0208

Before the addition of nanoparticles into the aqueous amine solution, 40 wt.% aqueous MDEA solution was investigated by introducing CO₂ into the equilibrium cell to study the CO₂ solubility. In this case, experiments were conducted at 303.15, 313.15, 323.15 and 333.15 K and results showed that the absorption capacity is decreased by increasing the temperature.

In order to evaluate the effect of nanoparticles on CO₂ absorption capacity, different concentration of GO was added to the aqueous MDEA solution. In this regard, 0.1 wt.%, 0.2 wt.%, 0.3 wt.% and 0.4 wt.% of GO nanoparticles were added to the solution and CO₂ solubility experiments were performed at 303.15 and 323.15 K. As shown in Fig .15, the results implied that CO₂ absorption increased as the nanoparticle dosage was increased to 0.2 wt.%. CO₂ absorption enhancement for concentration of 0.1 wt.% and 0.2 wt.% was measured to be up to 9.1% and 10.4%, respectively. Further addition of GO revealed no significant enhancement and even absorption capacity decreased in the case of 0.4 wt.% compared with nanoparticle-free MDEA solution.

Fig. 15

Stability of nanofluids is a key point that should be considered for the preparation of a stable solution containing nanoparticles. For this purpose, experiments were performed by addition of 0.1 wt.% of as-prepared nanostructure into the MDEA solution. In fact, dispersion occurs easily in a lower dosage of nanoparticles as well as the reactive sites on the surface of the nanoparticle are more active because of the slight viscosity altering. These reactive sites are more accessible to the gas molecules. Furthermore, Brownian motion is decreased in high concentrations of nanoparticles as blockage of the active sites and reduction of surface area. Blockages of the active sites raised from interparticle attraction and suppression of the particle motion increased the diffusion path length as well as decreased the mass transfer rate. In other words, the presence of a high concentration of nanoparticles in the solution makes a limitation for gas-liquid interactions. These phenomenon leads to a decrease in the absorption capacity of carbon dioxide. Based on these observations, we used 0.1 wt.% of nanoparticles as the optimal dosage for the next experiments [13,35,46,54,55].

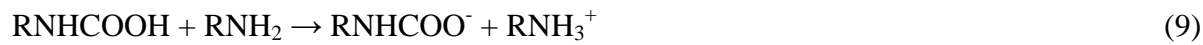
The influence of the nanoparticles toward CO₂ absorption capacity in nanofluids has been widely reported by researchers [56–60]. Different reasons have been suggested to justify the enhancement of CO₂ absorption capacity as a nanofluid is employed. Mass transfer coefficient will be improved as a nanoparticle is added to base fluid. Mass diffusion is mainly depended on the Brownian motion existence in the nanofluids [54]. This motion is a randomly and dynamically movement of nanoparticles in the base fluid. Shuttle or grazing effect is known as another reason for an explanation of mass transfer enhancement in the presence of nanostructured particles in a liquid phase. An additional amount of CO₂ can be transported to the liquid bulk via adsorption and desorption of nanoparticles. Adsorption and desorption are usually present in liquid diffusion layer and liquid bulk, respectively. Hydrodynamic effects are mainly created in the gas-liquid interface so that leads to a thinner diffusion layer and smaller gas bubbles desired for mass transfer phenomenon. As reported by Lewis and Whitman [61], the gas-liquid interface plays a critical role in transferring materials between gas and liquid phases. Furthermore, functional groups available on the surface of the nanoparticle can be considered due to the interactions between CO₂ and nanoparticles surface. In order to study the effect of functional groups on the CO₂ absorption capacity, we used amine-modified ZIF-90@GO in aqueous MDEA solution at the same temperatures and conditions.

Fig. 16 represents the absorption data for the addition of 0.1 wt.% of EDA@ZIF-90@GO into 40 wt.% of aqueous MDEA solution. Results indicated that the absorption capacity is decreased by increasing the temperature and increased by increasing the partial pressure. The absorption capacity was enhanced by up to 23% in the presence of EDA@ZIF-90@GO. The absorption capacity enhancement was relatively improved compared with the addition of GO into the amine solution.

Fig. 16

Therefore, the absorption capacity should be affected by another factor existence in the nanofluid properties. To understand the exact interactions occurred between CO₂ and reactive sites of nanoparticles, we suggest some reactions related to the amine functional groups. In fact, CO₂ is considered as an anionic component as introduced into a nanofluid so that interacts with some available amine functional groups (as a cationic component) and produce an intermediate. The generated intermediate deprotonates some intermediates that are

involved in generating protonated groups and carbamate on the surface of the amine-modified nanostructures [11]. The outcome is stabilizing the CO₂ on the nanoparticle surface according to the following reactions:



The collision between nanoparticles and gas bubbles in the fluid results in cracked bubbles with higher surface area and lower interface layer. These phenomenon's is subsequently associated with increased absorption ability of the nanofluid. The schematic of suggested mechanism occurred in the nanofluid toward CO₂ absorption has been presented in Fig. 17.

Fig. 17

3.3. Thermal conductivity

The base fluid for these experiments was considered as a 40 wt.% aqueous MDEA solution and then various nanoparticles were dispersed in the base fluid to investigate the thermal conductivity. Generally, nanofluids are more sensitive to temperature compared with the base fluid so that the effective thermal conductivity was increased in nanofluid by increasing the temperature. The effect of the temperature on the thermal conductivity of nanofluids was studied using a thermostat bath. The temperature range was varied from 298-328 K because of the absorption temperature employed in the absorption towers used in the refineries. Fig. 18 presents the effective thermal conductivity (K_{eff}) of the base fluid and nanofluids after addition of 0.1 wt.% of various nanoparticles into the base fluid. The experimental data confirm that thermal conductivity increases with raising the temperature. Addition of nanoparticles into the base fluid leads to an increase in thermal conductivity compared with the solution without the presence of the nanoparticles. The maximum thermal conductivity is related to the nanofluid containing SiO₂ compared with the base fluid. However, GO and amine modified GO increased the thermal conductivity and the increasing trend is continuously maintained with increasing the temperature.

Fig. 18

3.4. Convective heat transfer

In industrial sections, convective heat transfer is known as an important factor to develop the cooling processes, thermal convectors and power plants. Experimental data confirms that the convective heat transfer coefficient is improved for the nanofluids compared with solution without the presence of nanostructures. For this purpose, we added different dosage of amine modified GO into the base fluid. Different studies have focused on the convective heat transfer of nanofluids in the presence of metal oxides, but in this study, the effect of amine modified GO was investigated. As shown in Fig. 19, convective heat transfer of the as-prepared nanofluids with different dosage of the nanostructures (0.1, 0.2 and 0.3 wt.%) is enhanced (compared with the base fluid) by increasing the Reynolds number. Also, convective heat transfer coefficient is increased by increasing the nanoparticle concentration and the maximum convective heat transfer coefficient was observed in the nanofluid containing 0.3 wt.% of the nanoparticles. Generally, convective heat transfer coefficient of the nanofluids increased by 18-33% (in comparison with the base fluid) at different Reynolds numbers. Therefore, nanoparticles play an important role in enhancing the heat transfer properties of the fluids.

Fig. 19

4. Conclusions

In this study, different conditions were employed to study the CO₂ absorption using aqueous MDEA solution containing nanoparticles. EDA@ZIF-90@GO was synthesized and fully characterized by FTIR, XRD, BET, SEM and TGA techniques to understand the structure and properties. Zeta potential analysis was used to verify the stability of nanofluid and colloids in the mixture. GO was added to 40 wt.% aqueous MDEA solution in different concentrations. For addition of 0.1 and 0.2 wt.%, an absorption enhancement rate of 9.1% and 10.4% was observed respectively. Further addition of GO to the base fluid showed no significant improvement. When 0.1 wt.% of EDA@ZIF-90@GO was added to the base fluid, absorption capacity showed an enhancement rate of 23%. Temperature and pressure revealed a negative and positive effect on the absorption rate, respectively. Different factors are suggested to be involved in this enhancement rate including Brownian motion, grazing effect and shuttle effect. For amine functionalized nanocomposite, the further enhancement rate is assigned to the amine groups on the surface. Amine groups stabilize the CO₂ molecules resulted in the absorption rate. Heat transfer properties of the base fluid was improved after addition of nanoparticles.

Acknowledgment

The authors gratefully acknowledge the Iran National Science Foundation (INSF) for their kind supporting.

References

- [1] X. Wang, L. Chen, Q. Guo, Development of hybrid amine-functionalized MCM-41 sorbents for CO₂ capture, *Chem. Eng. J.* 260 (2015) 573–581.
doi:10.1016/j.cej.2014.08.107.
- [2] M. Irani, K.A.M. Gasem, B. Dutcher, M. Fan, CO₂ capture using nanoporous TiO_(OH)₂/tetraethylenepentamine, *Fuel.* 183 (2016) 601–608.
doi:10.1016/j.fuel.2016.06.129.
- [3] T. Wang, J. Liu, H. Huang, M. Fang, Z. Luo, Preparation and kinetics of a heterogeneous sorbent for CO₂ capture from the atmosphere, *Chem. Eng. J.* (2016).
doi:10.1016/j.cej.2015.09.009.
- [4] N.A. Rashidi, S. Yusup, An overview of activated carbons utilization for the post-combustion carbon dioxide capture, *J. CO₂ Util.* 13 (2016) 1–16.
doi:10.1016/j.jcou.2015.11.002.
- [5] T. Best, K.N. Finney, D.B. Ingham, M. Pourkashanian, CO₂-enhanced and humidified operation of a micro-gas turbine for carbon capture, *J. Clean. Prod.* 176 (2018) 370–381. doi:10.1016/j.jclepro.2017.12.062.
- [6] J.W. Lee, I. Torres Pineda, J.H. Lee, Y.T. Kang, Combined CO₂absorption/regeneration performance enhancement by using nanoabsorbents, *Appl. Energy.* 178 (2016) 164–176. doi:10.1016/j.apenergy.2016.06.048.
- [7] F. Banat, O. Younas, I. Didarul, Energy and exergical dissection of a natural gas sweetening plant using methyldiethanol amine (MDEA) solution, *J. Nat. Gas Sci. Eng.* (2014). doi:10.1016/j.jngse.2013.10.005.
- [8] P.Y. Chung, A.N. Soriano, R.B. Leron, M.H. Li, Equilibrium solubility of carbon dioxide in the amine solvent system of (triethanolamine + piperazine + water), *J.*

- Chem. Thermodyn. (2010). doi:10.1016/j.jct.2010.02.005.
- [9] S.K. Dash, S.S. Bandyopadhyay, Studies on the effect of addition of piperazine and sulfolane into aqueous solution of N-methyldiethanolamine for CO₂ capture and VLE modelling using eNRTL equation, Int. J. Greenh. Gas Control. 44 (2016) 227–237. doi:10.1016/j.ijggc.2015.11.007.
- [10] A. Maleki, V. Irani, A. Tavasoli, M. Vahidi, Enhancement of CO₂ solubility in a mixture of 40 wt% aqueous N-Methyldiethanolamine solution and diethylenetriamine functionalized graphene oxide, J. Nat. Gas Sci. Eng. (n.d.). doi:<https://doi.org/10.1016/j.jngse.2018.04.032>.
- [11] V. Irani, A. Tavasoli, M. Vahidi, Preparation of amine functionalized reduced graphene oxide / methyl diethanolamine nanofluid and its application for improving the CO₂ and H₂S absorption, J. Colloid Interface Sci. (n.d.). doi:<https://doi.org/10.1016/j.jcis.2018.05.018>.
- [12] V. Irani, A. Tavasoli, A. Maleki, M. Vahidi, Polyethyleneimine-functionalized HKUST-1/MDEA nanofluid to enhance the absorption of CO₂in gas sweetening process, Int. J. Hydrogen Energy. 43 (2018) 5610–5619. doi:10.1016/j.ijhydene.2018.01.120.
- [13] V. Irani, A. Maleki, A. Tavasoli, CO₂ absorption enhancement in graphene-oxide/MDEA nanofluid, J. Environ. Chem. Eng. 7 (2019) 102782. doi:<https://doi.org/10.1016/j.jece.2018.11.027>.
- [14] A. Maleki, V. Irani, A. Tavasoli, H₂S solubility enhancement using ethylene diamine functionalized carbon nanotubes and the aqueous solution of N-methyldiethanolamine, J. Nat. Gas Sci. Eng. 71 (2019) 103004. doi:<https://doi.org/10.1016/j.jngse.2019.103004>.
- [15] R. Aghehrochaboki, Y. Aghdoud, S. Arash, V. Irani, Journal of Environmental Chemical Engineering Polyethyleneimine functionalized graphene oxide / methyldiethanolamine nanofluid : Preparation , characterization , and investigation of CO₂ absorption, J. Environ. Chem. Eng. 7 (2019) 103285. doi:10.1016/j.jece.2019.103285.
- [16] M. Vahidi, A. Tavasoli, A.M. Rashidi, Preparation of amine functionalized UiO-66,

- mixing with aqueous N-Methyldiethanolamine and application on CO₂ solubility, *J. Nat. Gas Sci. Eng.* 28 (2016) 651–659. doi:10.1016/j.jngse.2015.11.050.
- [17] W. Jung, J. Park, K.S. Lee, Kinetic modeling of CO₂ adsorption on an amine-functionalized solid sorbent, *Chem. Eng. Sci.* 177 (2018) 122–131. doi:10.1016/j.ces.2017.11.003.
- [18] L.A. Darunte, K.S. Walton, D.S. Sholl, C.W. Jones, CO₂ capture via adsorption in amine-functionalized sorbents, *Curr. Opin. Chem. Eng.* 12 (2016). doi:10.1016/j.coche.2016.03.002.
- [19] L.A. Darunte, K.S. Walton, D.S. Sholl, C.W. Jones, CO₂ capture via adsorption in amine-functionalized sorbents, *Curr. Opin. Chem. Eng.* 12 (2016) 82–90. doi:10.1016/j.coche.2016.03.002.
- [20] M.J. Al-Marri, M.M. Khader, M. Tawfik, G. Qi, E.P. Giannelis, CO₂ sorption kinetics of scaled-up polyethylenimine-functionalized mesoporous silica sorbent, *Langmuir*. 31 (2015). doi:10.1021/acs.langmuir.5b00189.
- [21] J. Yu, L.-H. Xie, J.-R. Li, Y. Ma, J.M. Seminario, P.B. Balbuena, CO₂ Capture and Separations Using MOFs: Computational and Experimental Studies, *Chem. Rev.* 117 (2017). doi:10.1021/acs.chemrev.6b00626.
- [22] S. Chowdhury, R. Balasubramanian, Three-Dimensional Graphene-Based Porous Adsorbents for Postcombustion CO₂ Capture, *Ind. Eng. Chem. Res.* 55 (2016). doi:10.1021/acs.iecr.5b04052.
- [23] P. Nugent, Y. Belmabkhout, S.D. Burd, A.J. Cairns, R. Luebke, K. Forrest, T. Pham, S.Q. Ma, B. Space, L. Wojtas, M. Eddaoudi, M.J. Zaworotko, Porous materials with optimal adsorption thermodynamics and kinetics for CO₂ separation, *Nature*. 495 (2013). doi:10.1038/nature11893.
- [24] D.M. D'Alessandro, B. Smit, J.R. Long, Carbon dioxide capture: Prospects for new materials, *Angew. Chemie - Int. Ed.* 49 (2010) 6058–6082. doi:10.1002/anie.201000431.
- [25] E.E. Ünveren, B.Ö. Monkul, Ş. Sarıoğlu, N. Karademir, E. Alper, Solid amine sorbents for CO₂ capture by chemical adsorption: A review, 3 (2017) 37–50. doi:10.1016/j.petlm.2016.11.001.

- [26] L. Guo, J. Yang, G. Hu, X. Hu, H. DaCosta, M. Fan, CO₂ removal from flue gas with amine-impregnated titanate nanotubes, *Nano Energy.* 25 (2016) 1–8. doi:10.1016/j.nanoen.2016.04.038.
- [27] J. Song, X. Wang, C.-T. Chang, J. Song, X. Wang, C.-T. Chang, Preparation and Characterization of Graphene Oxide, *J. Nanomater.* 2014 (2014) 1–6. doi:10.1155/2014/276143.
- [28] S.Y. Lee, S.J. Park, A review on solid adsorbents for carbon dioxide capture, *J. Ind. Eng. Chem.* 23 (2015). doi:10.1016/j.jiec.2014.09.001.
- [29] A.E. Creamer, B. Gao, Carbon-based adsorbents for postcombustion CO₂ capture: A critical review, *Environ. Sci. Technol.* 50 (2016). doi:10.1021/acs.est.6b00627.
- [30] T. Kuila, S. Bose, A.K. Mishra, P. Khanra, N.H. Kim, J.H. Lee, Chemical functionalization of graphene and its applications, *Prog. Mater. Sci.* 57 (2012) 1061–1105. doi:10.1016/j.pmatsci.2012.03.002.
- [31] Y. Cao, Y. Zhao, Z. Lv, F. Song, Q. Zhong, Preparation and enhanced CO₂ adsorption capacity of UiO-66/graphene oxide composites, *J. Ind. Eng. Chem.* 27 (2015) 102–107. doi:10.1016/j.jiec.2014.12.021.
- [32] C. Petit, J. Burress, T.J. Bandosz, The synthesis and characterization of copper-based metal – organic framework / graphite oxide composites, *Carbon N. Y.* 49 (2010) 563–572. doi:10.1016/j.carbon.2010.09.059.
- [33] S. Xian, F. Xu, C. Ma, Y. Wu, Q. Xia, H. Wang, Z. Li, Vapor-enhanced CO₂ adsorption mechanism of composite PEI@ZIF-8 modified by polyethyleneimine for CO₂/N₂ separation, *Chem. Eng. J.* 280 (2015) 363–369. doi:10.1016/j.cej.2015.06.042.
- [34] D.K. Devendiran, V.A. Amirtham, A review on preparation, characterization, properties and applications of nanofluids, *Renew. Sustain. Energy Rev.* 60 (2016) 21–40. doi:10.1016/j.rser.2016.01.055.
- [35] L. Fang, H. Liu, Y. Bian, Y. Liu, Y. Yang, Experimental Study on Enhancement of Bubble Absorption of Gaseous CO₂ with Nanofluids in Ammonia, *J. Harbin Inst. Technol. (New Ser.)* 24 (2017) 80–86. doi:10.11916/j.issn.1005-9113.15246.
- [36] W. Zhang, J. Ma, D. Gao, Y. Zhou, C. Li, J. Zha, J. Zhang, Preparation of amino-

- functionalized graphene oxide by Hoffman rearrangement and its performances on polyacrylate coating latex, *Prog. Org. Coatings.* 94 (2016) 9–17.
doi:10.1016/j.porgcoat.2016.01.013.
- [37] D. Saha, S. Deng, Synthesis, characterization and hydrogen adsorption in mixed crystals of MOF-5 and MOF-177, *Int. J. Hydrogen Energy.* 34 (2009) 2670–2678.
doi:10.1016/j.ijhydene.2009.01.082.
- [38] S. Leaper, A. Abdel-Karim, B. Faki, J.M. Luque-Alled, M. Alberto, A. Vijayaraghavan, S.M. Holmes, G. Szekely, M.I. Badawy, N. Shokri, P. Gorgojo, Flux-enhanced PVDF mixed matrix membranes incorporating APTS-functionalized graphene oxide for membrane distillation, *J. Memb. Sci.* 554 (2018) 309–323.
doi:10.1016/j.memsci.2018.03.013.
- [39] Y. Lin, H. Lin, H. Wang, Y. Suo, B. Li, C. Kong, L. Chen, Enhanced selective CO₂ adsorption on polyamine/MIL-101(Cr) composites, *J. Mater. Chem. A.* 2 (2014).
doi:10.1039/C4TA01174K.
- [40] M. Shokouhi, H. Bozorgzade, P. Sattari, Solubility of Hydrogen Sulfide in Aqueous Blends of 2-Amino-2-methyl-1-propanol and N -Methyldiethanolamine: Experimental Measurement and Modeling, *J. Chem. Eng. Data.* 60 (2015) 2119–2127.
doi:10.1021/acs.jced.5b00194.
- [41] M. Shokouhi, A.T. Zoghi, M. Vahidi, B. Moshtari, Solubility of carbon dioxide in aqueous blends of 2-amino-2-methyl-1-propanol and N-methyldiethanolamine, *J. Chem. Eng. Data.* 60 (2015) 1250–1258. doi:10.1021/je500860v.
- [42] M. Shokouhi, A.R. Rezaierad, S.M. Zekordi, M. Abbasghorbani, M. Vahidi, Solubility of Hydrogen Sulfide in Ethanediol, 1,2-Propanediol, 1-Propanol, and 2-Propanol: Experimental Measurement and Modeling, *J. Chem. Eng. Data.* 61 (2016) 512–524.
doi:10.1021/acs.jced.5b00680.
- [43] M.H. Jenab, M. Vahidi, M. Mehrabi, Solubility of Carbon Dioxide in Aqueous Mixtures of DIPA + MDEA and DIPA + PZ Solutions, *J. Chinese Chem. Soc.* 53 (2006) 283–286. doi:10.1002/jccs.200600034.
- [44] M.H. Jenab, M.A. Abdi, S.H. Najibi, M. Vahidi, N.S. Matin, N. Iranian, O. Company, Solubility of Carbon Dioxide in Aqueous Mixtures of, *Engineering.* (2005) 583–586.

- doi:10.1021/je049666p.
- [45] M.K. Park, O.C. Sandall, Solubility of carbon dioxide and nitrous oxide in 50 mass % methyldiethanolamine, *J. Chem. Eng. Data.* 46 (2001) 166–168.
doi:10.1021/je000190t.
- [46] A. Arshad, M. Jabbal, Y. Yan, D. Reay, A review on graphene based nanofluids : Preparation , characterization and applications Particle size Synthesis method Preparation method Distilled water Liquid paraffin, Elsevier B.V., 2019.
doi:10.1016/j.molliq.2019.01.153.
- [47] Y. Lin, C. Kong, L. Chen, Amine-functionalized metal–organic frameworks: structure, synthesis and applications, *RSC Adv.* 6 (2016) 32598–32614.
doi:10.1039/C6RA01536K.
- [48] J. Pokhrel, N. Bhoria, S. Anastasiou, T. Tsou, Microporous and Mesoporous Materials CO 2 adsorption behavior of amine-functionalized ZIF-8 , graphene oxide , and ZIF-8 / graphene oxide composites under dry and wet conditions, 267 (2018) 53–67.
doi:10.1016/j.micromeso.2018.03.012.
- [49] D.V. Quang, T.A. Hatton, M.R.M. Abu-Zahra, Thermally Stable Amine-Grafted Adsorbent Prepared by Impregnating 3-Aminopropyltriethoxysilane on Mesoporous Silica for CO₂ Capture, *Ind. Eng. Chem. Res.* 55 (2016) 7842–7852.
doi:10.1021/acs.iecr.5b04096.
- [50] R. Ben-Mansour, M.A. Habib, O.E. Bamidele, M. Basha, N.A.A. Qasem, A. Peedikakkal, T. Laoui, M. Ali, Carbon capture by physical adsorption: Materials, experimental investigations and numerical modeling and simulations - A review, *Appl. Energy.* 161 (2016) 225–255. doi:10.1016/j.apenergy.2015.10.011.
- [51] B. Szczęśniak, J. Choma, M. Jaroniec, Gas adsorption properties of hybrid graphene-MOF materials, *J. Colloid Interface Sci.* 514 (2018) 801–813.
doi:10.1016/j.jcis.2017.11.049.
- [52] K.-P. Shen, M.-H. Li, Solubility of Carbon Dioxide in Aqueous Mixtures of Monoethanolamine with Methyldiethanolamine, *J. Chem. Eng. Data.* 37 (1992) 96–100. doi:10.1021/je00005a025.
- [53] S. Ma'mun, R. Nilsen, H.F. Svendsen, O. Juliussen, Solubility of carbon dioxide in 30

- mass % monoethanolamine and 50 mass % methyldiethanolamine solutions, *J. Chem. Eng. Data.* 50 (2005) 630–634. doi:10.1021/je0496490.
- [54] H. Mohammadoost, A. Azari, M. Ansarpour, S. Osfouri, Experimental investigation of CO₂removal from N₂by metal oxide nanofluids in a hollow fiber membrane contactor, *Int. J. Greenh. Gas Control.* 69 (2018) 60–71.
doi:10.1016/j.ijggc.2017.12.012.
- [55] J.W. Lee, Y.T. Kang, CO₂ absorption enhancement by Al₂O₃ nanoparticles in NaCl aqueous solution, *Energy.* 53 (2013) 206–211.
doi:<https://doi.org/10.1016/j.energy.2013.02.047>.
- [56] Y. Xuan, Conception for enhanced mass transport in binary nanofluids, *Heat Mass Transf.* 46 (2009) 277. doi:10.1007/s00231-009-0564-z.
- [57] J. Saien, H. Bamdadi, Mass Transfer from Nanofluid Single Drops in Liquid–Liquid Extraction Process, *Ind. Eng. Chem. Res.* 51 (2012) 5157–5166.
doi:10.1021/ie300291k.
- [58] M. Nabipour, P. Keshavarz, S. Raeissi, Enquête expérimentale portant sur l'absorption du CO₂dans les nanofluides Fe₃O₄et MWCNT à base de Sulfinol-M, *Int. J. Refrig.* 73 (2017) 1–10. doi:10.1016/j.ijrefrig.2016.09.010.
- [59] I.T. Pineda, C.K. Choi, Y.T. Kang, CO₂gas absorption by CH₃OH based nanofluids in an annular contactor at low rotational speeds, *Int. J. Greenh. Gas Control.* 23 (2014) 105–112. doi:10.1016/j.ijggc.2014.02.008.
- [60] M. Darabi, M. Rahimi, A. Molaei Dehkordi, Gas absorption enhancement in hollow fiber membrane contactors using nanofluids: Modeling and simulation, *Chem. Eng. Process. Process Intensif.* 119 (2017) 7–15.
doi:<https://doi.org/10.1016/j.cep.2017.05.007>.
- [61] C. Pang, W. Wu, W. Sheng, H. Zhang, Y.T. Kang, Mass transfer enhancement by binary nanofluids (NH₃/H₂O + Ag nanoparticles) for bubble absorption process, *Int. J. Refrig.* 35 (2012) 2240–2247. doi:10.1016/j.ijrefrig.2012.08.006.

Figure Captions

Fig. 1. Reaction schematic for preparation of ZIF-90.

Fig. 2. Schematic of APTES functionalization of GO.

Fig. 3. Schematic of ZIF-90 functionalization of GO.

Fig. 4. Schematic of EDA functionalization of ZIF-90@GO.

Fig. 5. A schematic structure of the system including the equilibrium cell, gas container, gas reservoir, water bath, and estimation instruments.

Fig. 6. Schematic design of the convective heat transfer measurement system.

Fig. 7. Zeta potential diagram of 40 wt.% aqueous MDEA solution in the presence of 0.1 wt.% EDA@ZIF-90@GO.

Fig. 8. XRD patterns of ZIF-90, GO, ZIF-90@APTES-GO and EDA@ZIF-90-GO.

Fig. 9. FTIR spectra of (a) GO, (b) APTES-GO, (c) ZIF-90@APTES-GO, and (d) EDA@ZIF-90@APTES-GO.

Fig. 10. SEM images of the (a) GO, (b) APTES functionalized GO, (c) ZIF-90@APTES-GO, and (d) EDA-ZIF-90@APTES-GO.

Fig. 11. N₂ adsorption-desorption of ZIF-90@APTES-GO and EDA-ZIF-90@APTES-GO to study the BET surface area and pore size of samples.

Fig. 12. Thermal behavior (TGA) of ZIF-90, GO, ZIF-90@GO and EDA@ZIF-90@GO.

Fig. 13. Comparison of our results with data available in the literature at reaction temperature of 313.15 K.

Fig. 14. Comparison of our results with data available in the literature at reaction temperature of 328.15 and 343.15 K.

Fig. 15. The results of CO₂ absorption experiments obtained from three separate solutions of 40 wt.% MDEA, 40 wt. % MDEA + 0.1 wt.% GO and 40 wt.% MDEA + 0.2 wt.% GO at (A) 303.15 and (B) 323.15 K.

Fig. 16. CO₂ absorption data in (40 wt.% MDEA) and (40 wt.% MDEA + 0.1 wt.% EDA@ZIF-90@GO) at (A) 303.15, (B) 313.15, (C) 323.15, and (D) 333.15 K.

Fig. 17. Schematic of the absorption enhancement via cracked bubbles and increased surface area in the presence of nanoparticles.

Fig. 18. Effective thermal conductivity of different nanofluids and base fluid at different temperatures.

Fig. 19. Variation of convective heat transfer coefficient in the presence of different dosage of amine modified GO and Reynolds numbers.

Figures

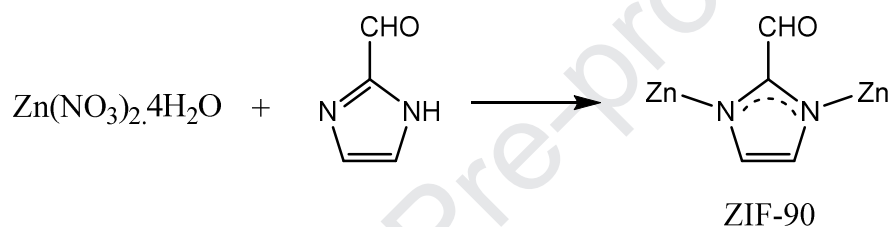


Fig. 1

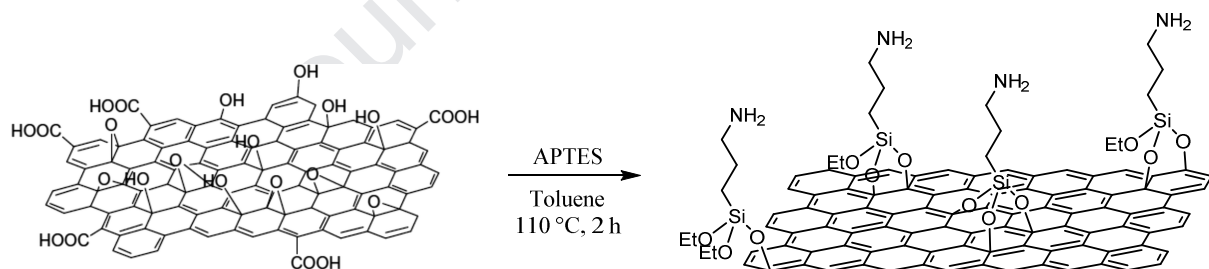
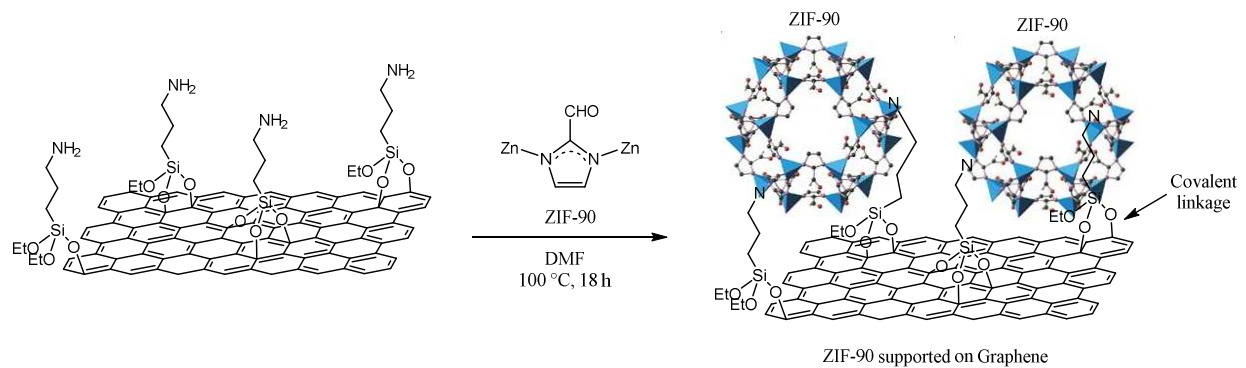
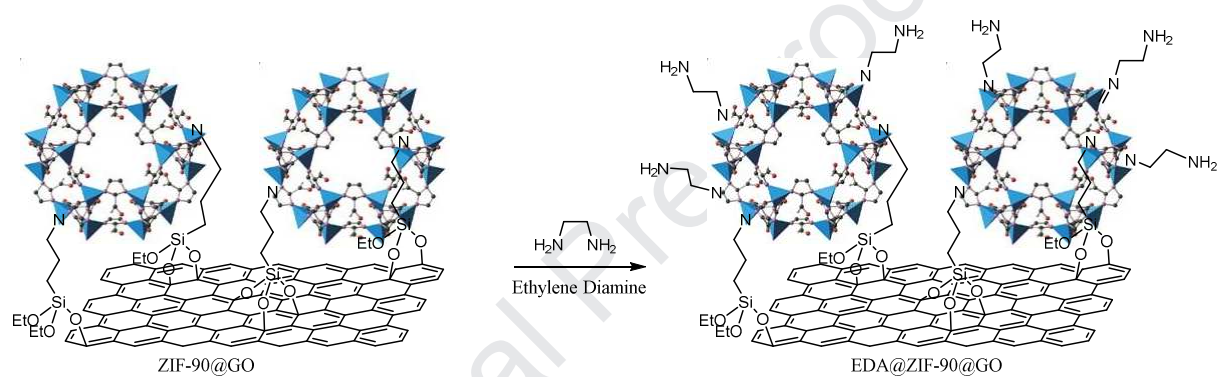


Fig. 2

**Fig. 3****Fig. 4**

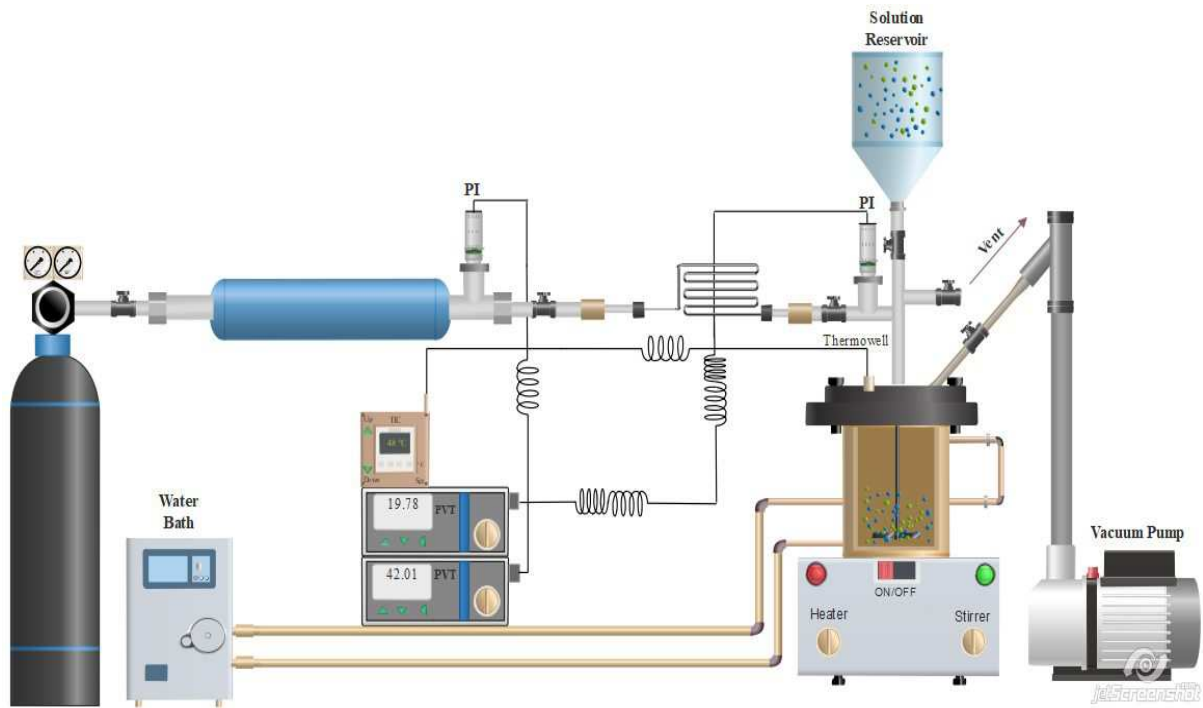


Fig. 5

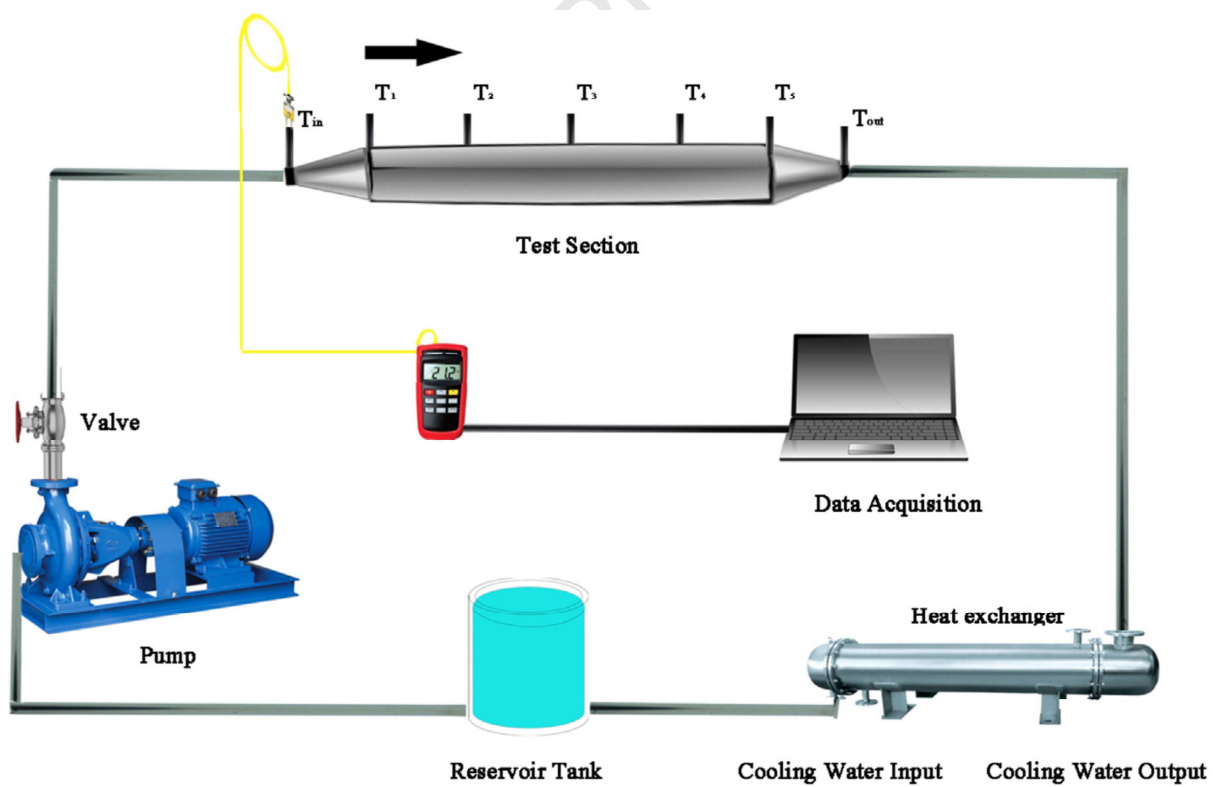


Fig. 6

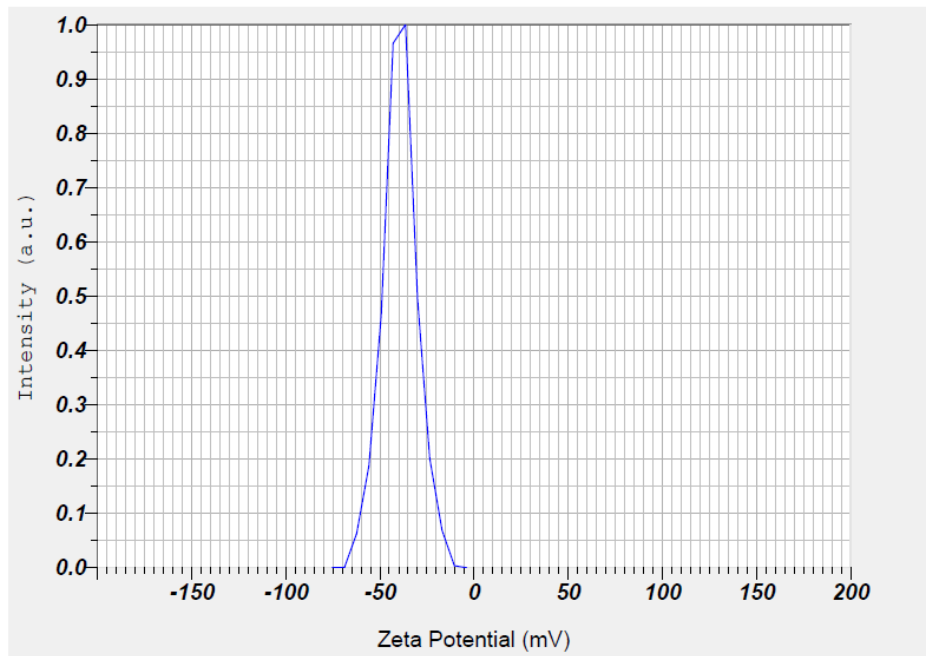


Fig. 7

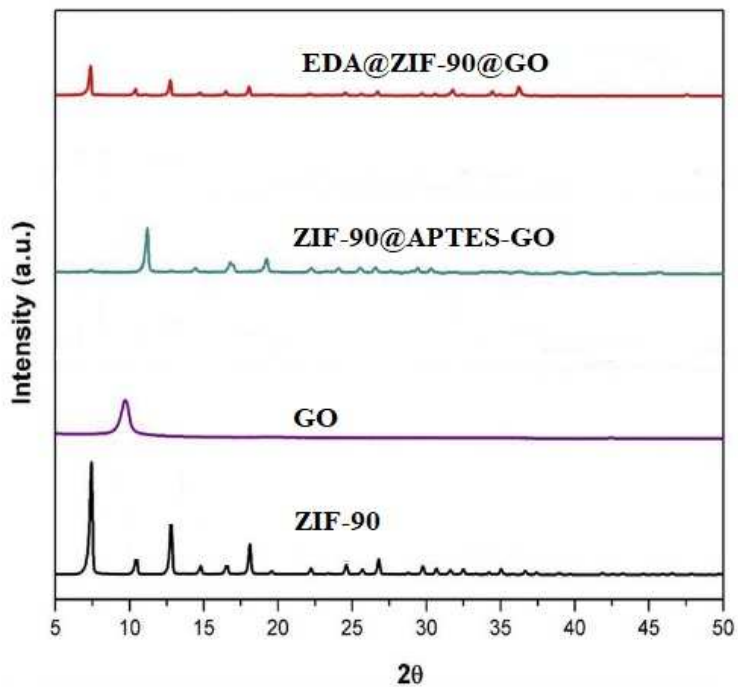


Fig. 8

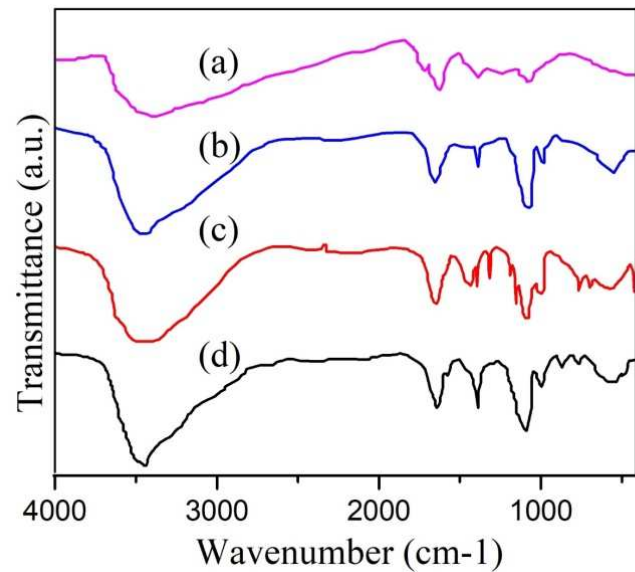


Fig. 9

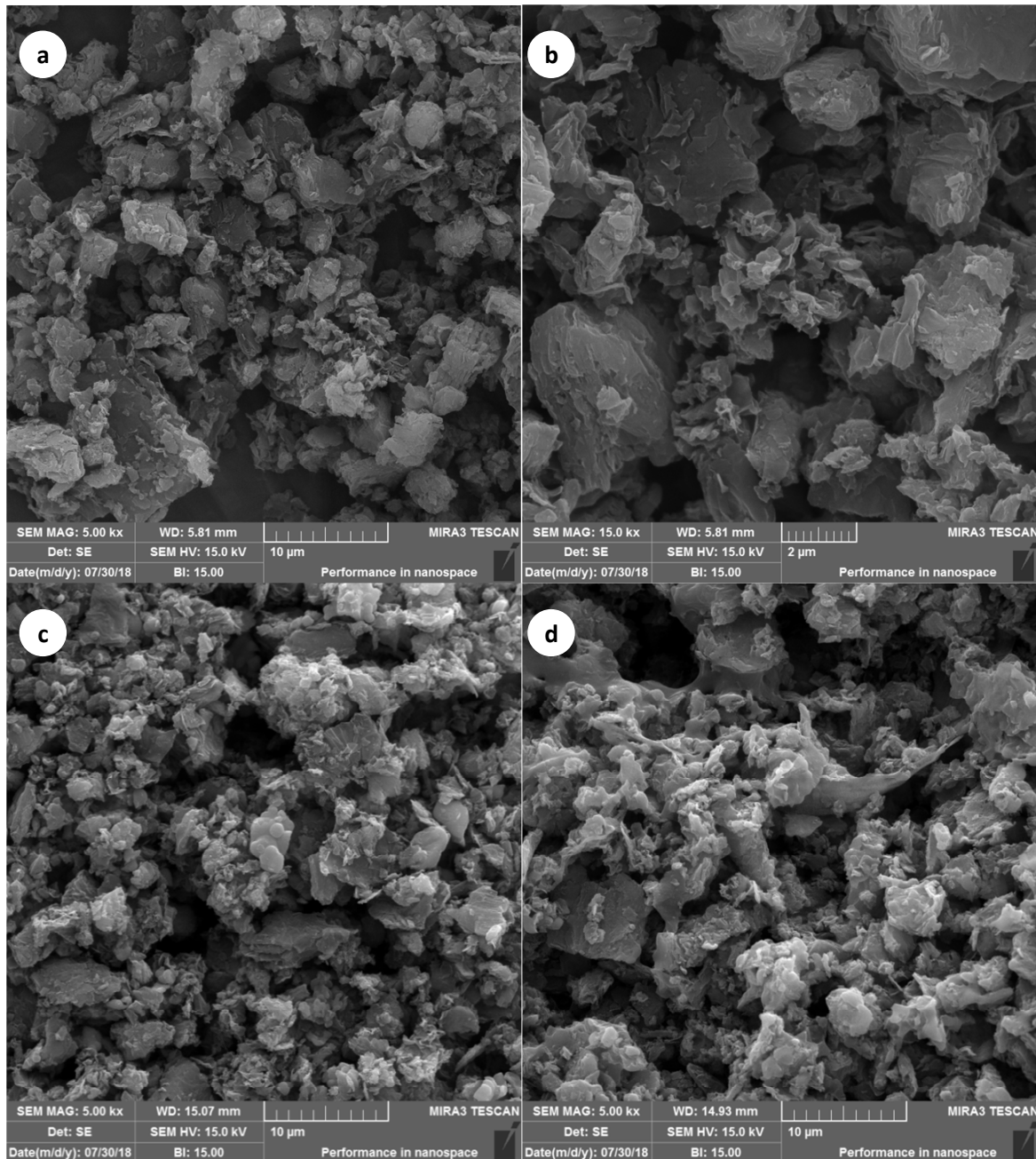
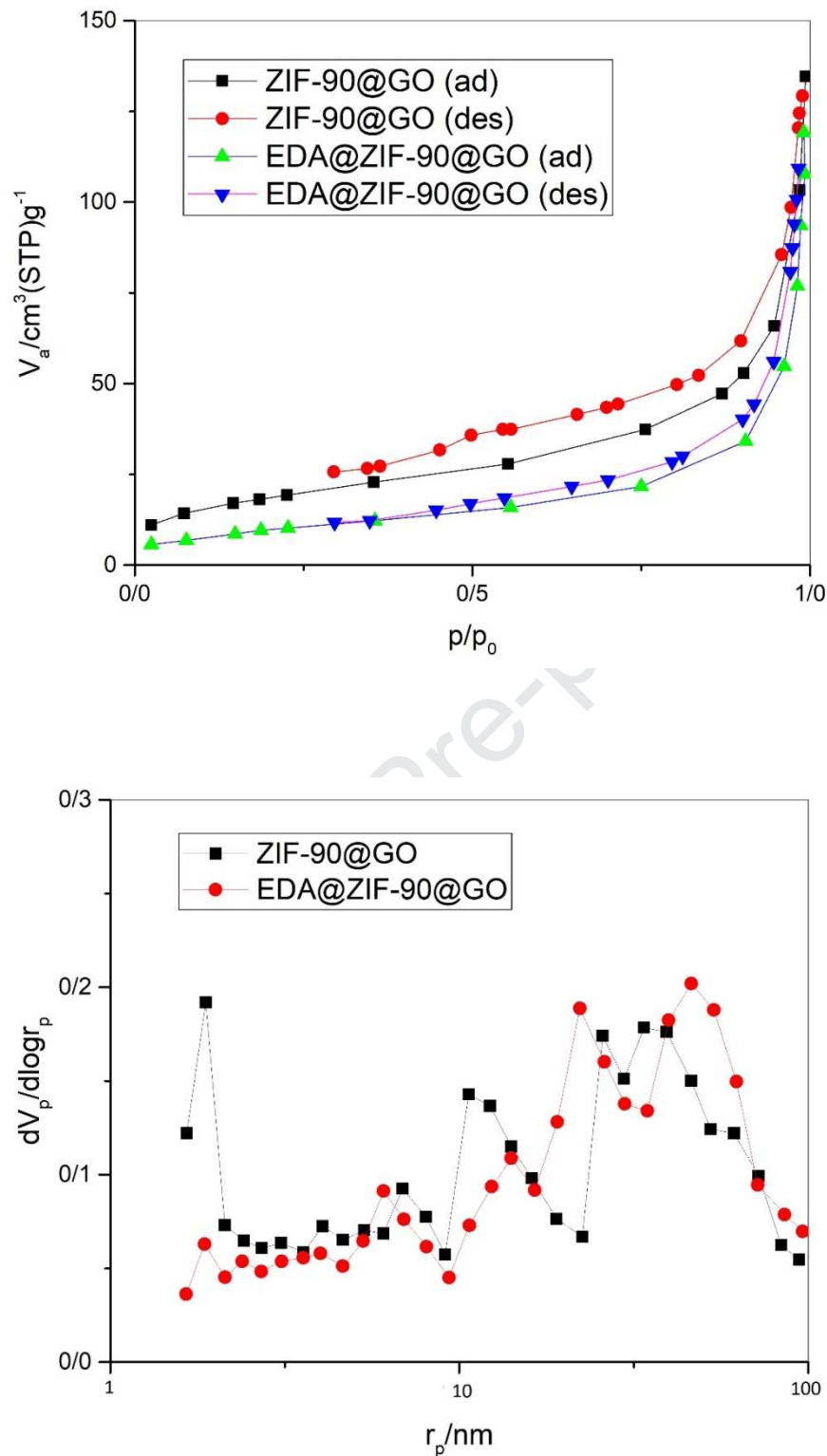


Fig. 10

**Fig. 11**

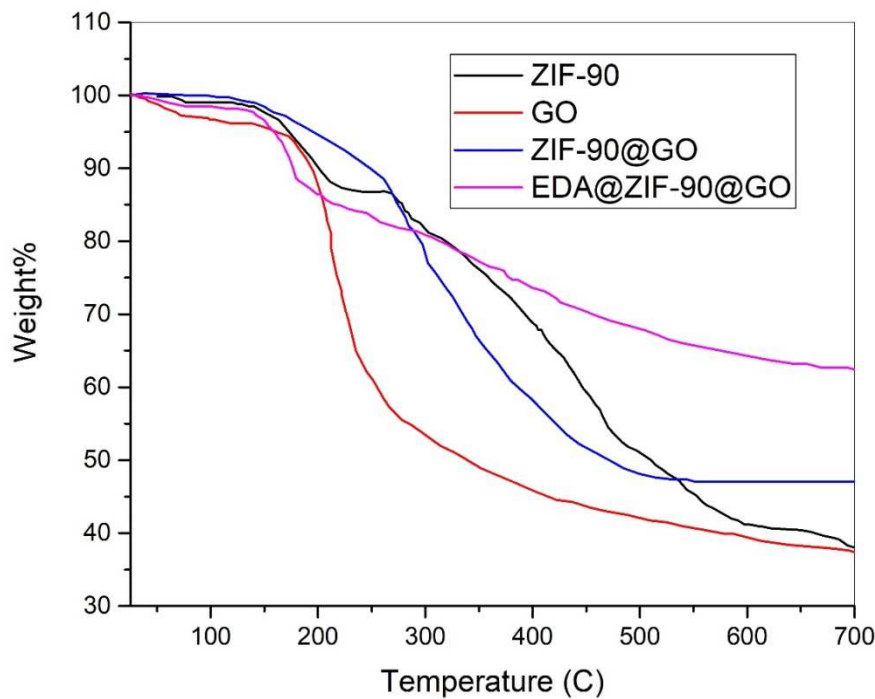


Fig. 12

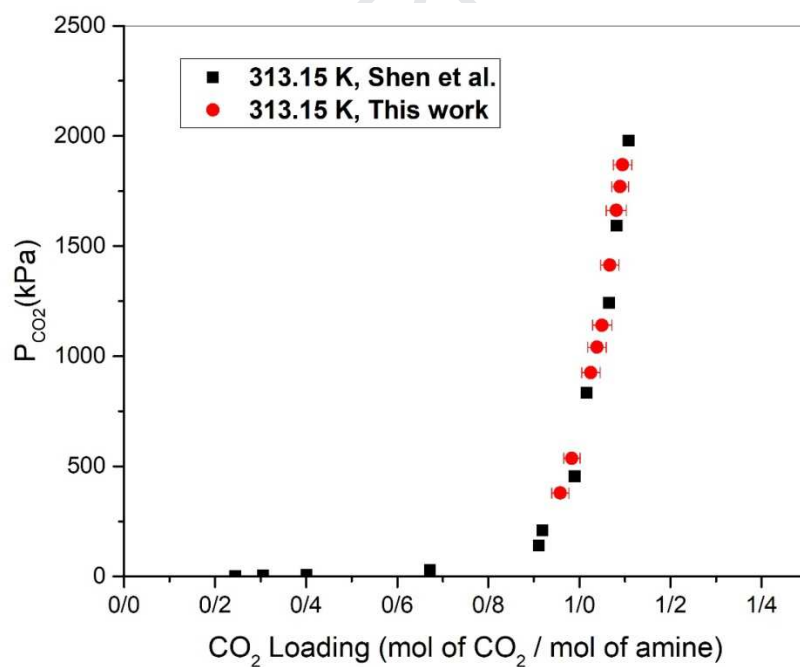


Fig. 13

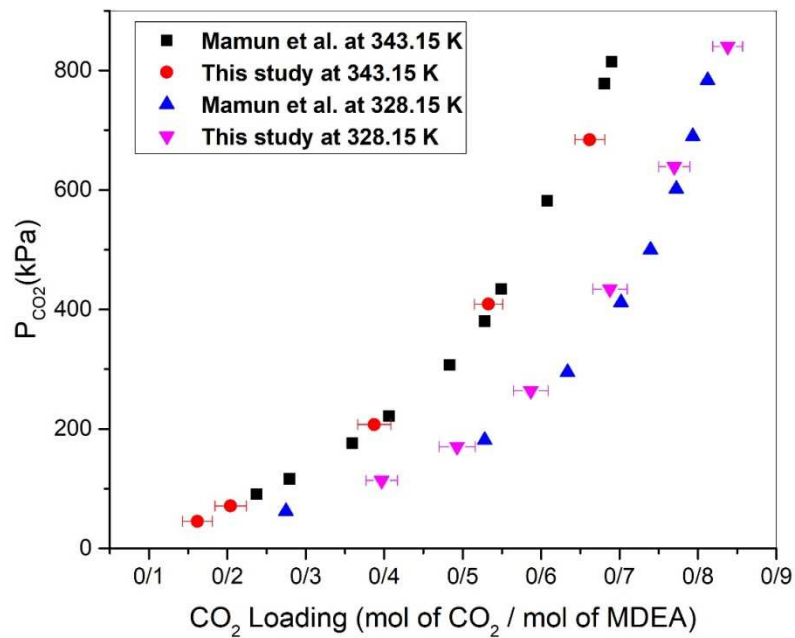
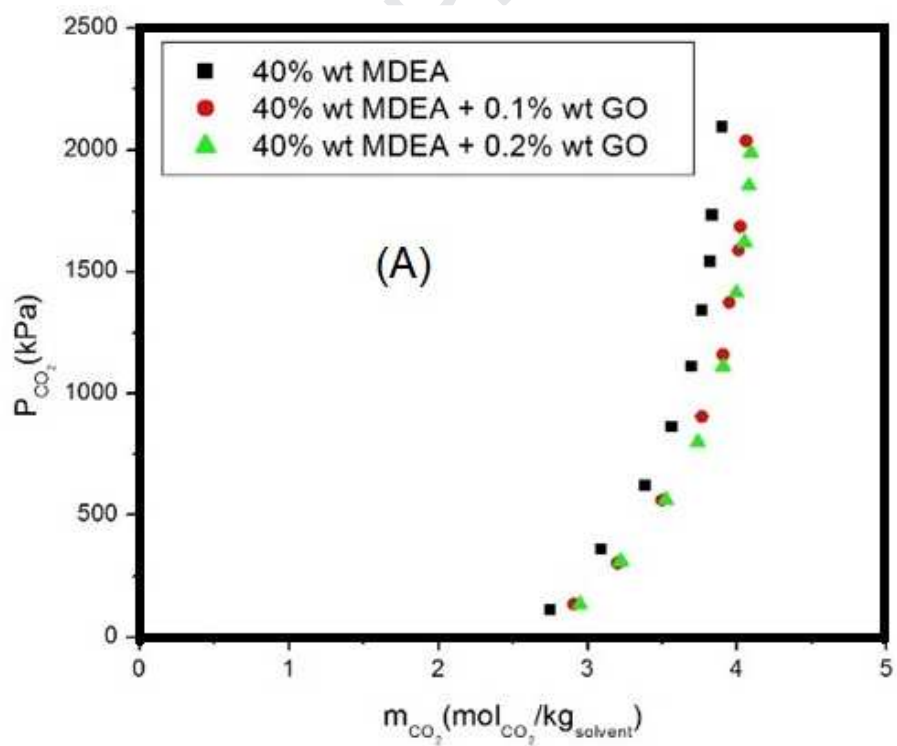


Fig. 14



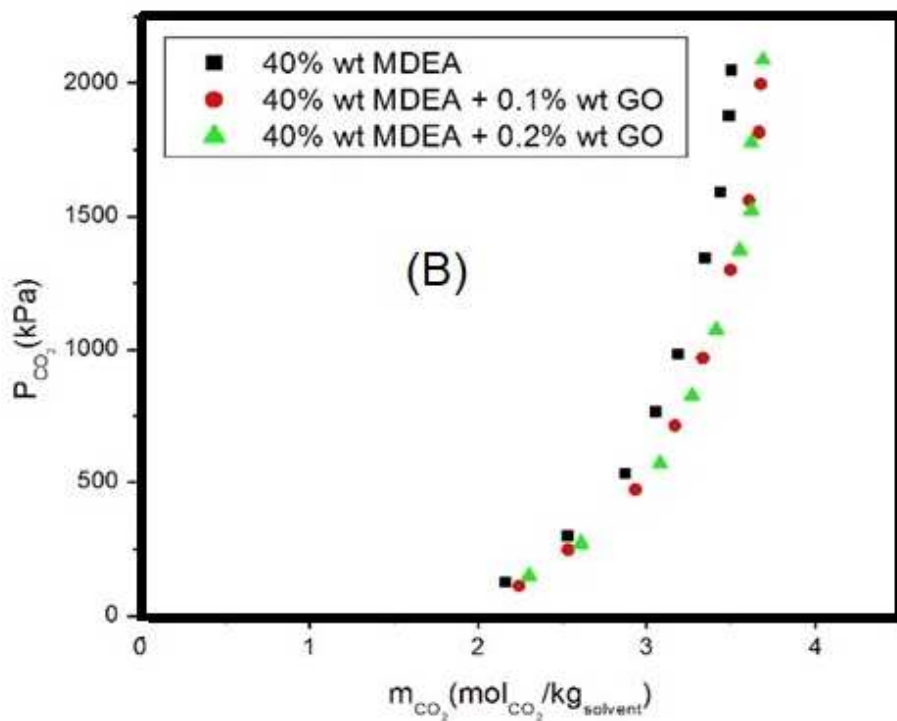
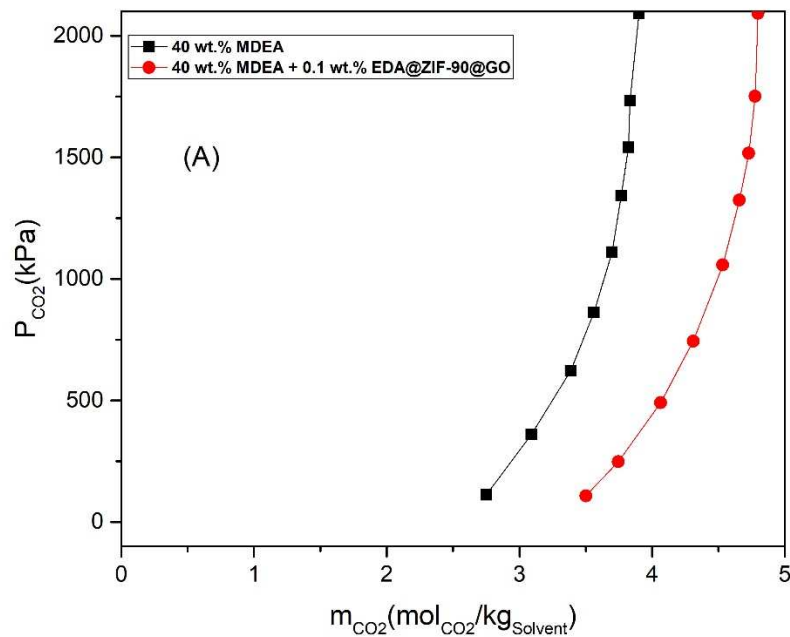
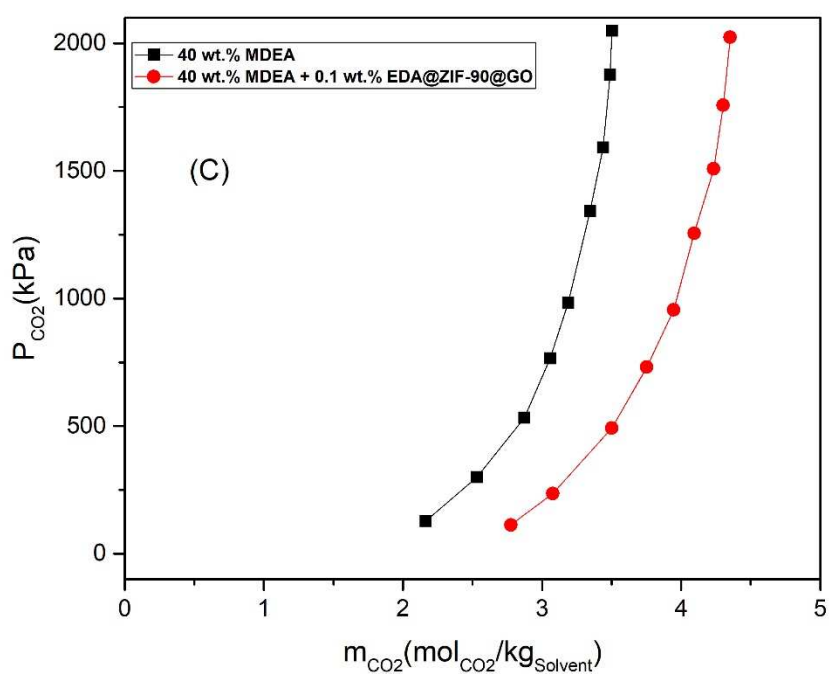
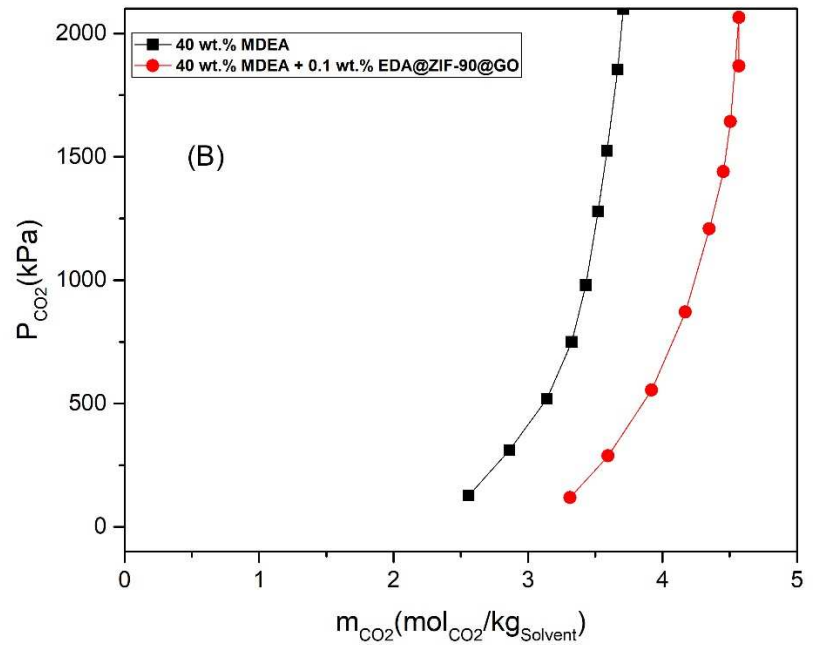


Fig. 15





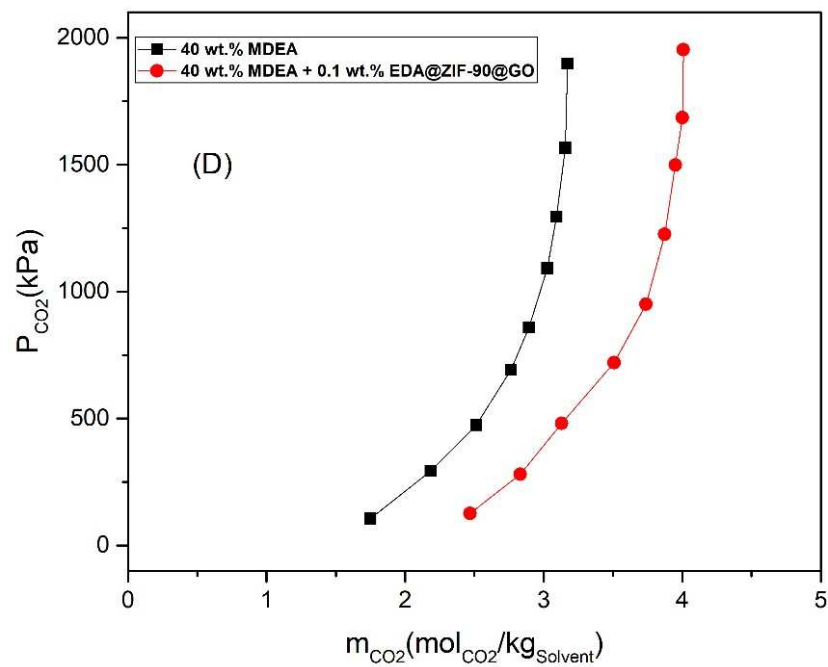


Fig. 16

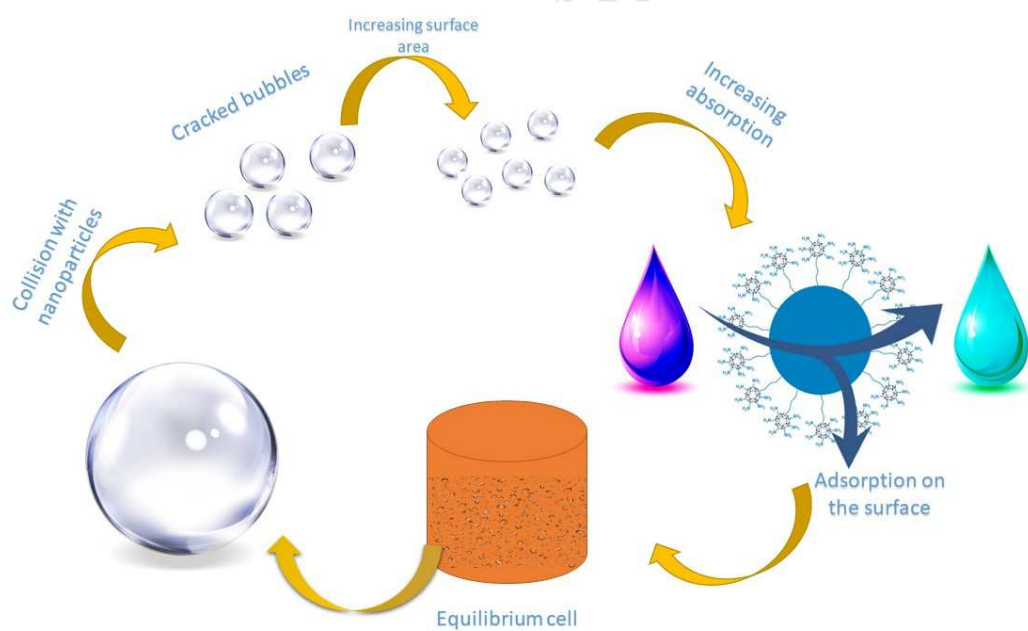


Fig. 17

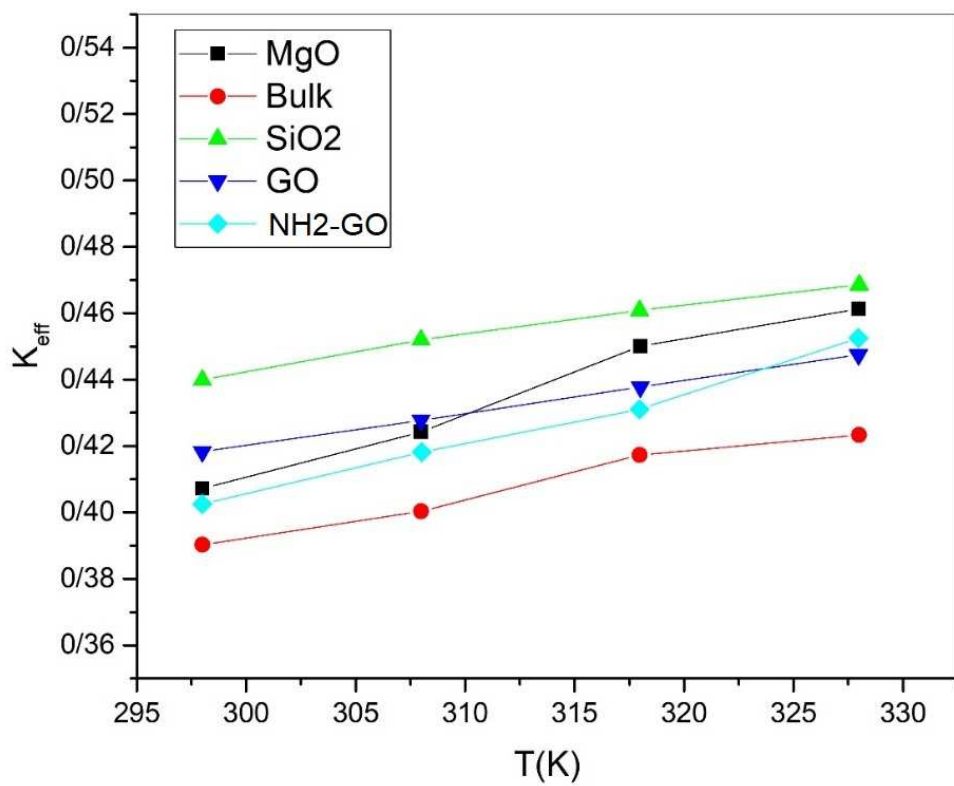


Fig. 18

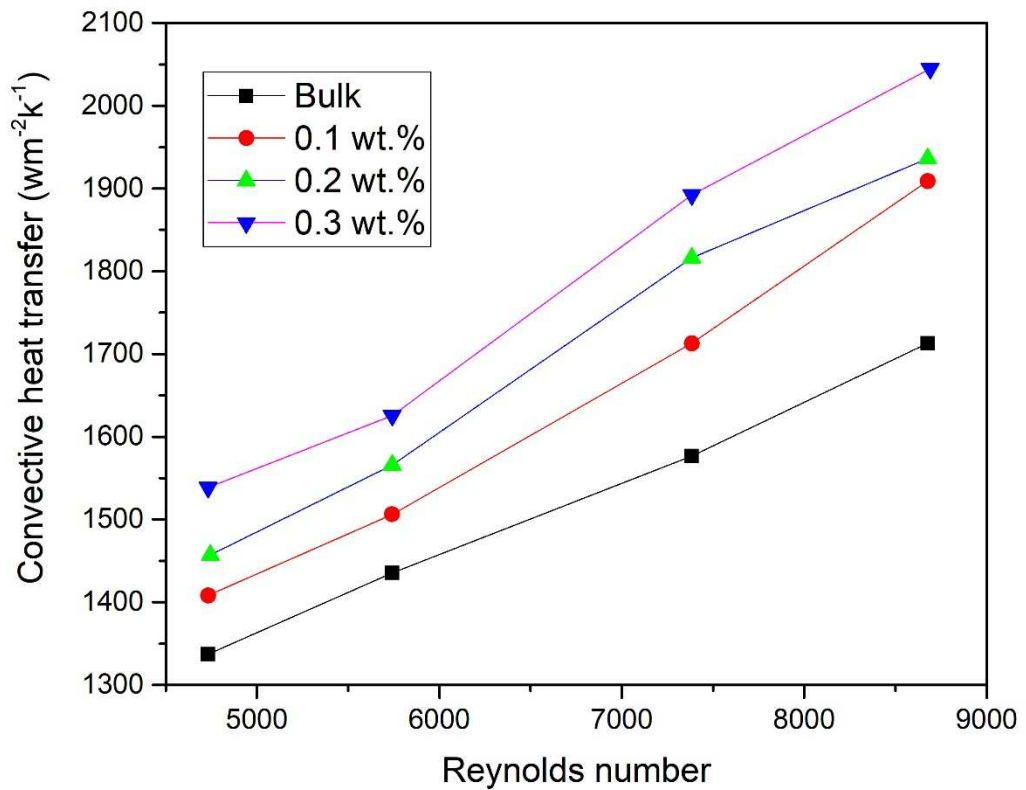


Fig. 19

Highlights

- A novel method was investigated to improve the CO₂ absorption enhancement.
- ZIF-90@APTES-GO was synthesized and functionalized with amine groups.
- EDA@ZIF-90@GO was added to the 40 wt.% aqueous MDEA solution.
- CO₂ absorption was enhanced up to 23% in the presence of 0.1 wt.% of nanoparticles.

Declaration of interests

The authors declare that they have no known competing financial interests or personal relationships that could have appeared to influence the work reported in this paper.

The authors declare the following financial interests/personal relationships which may be considered as potential competing interests: